2016

The transition from the open minimum to the ring minimum on the ground state and on the lowest excited state of like symmetry in ozone: A configuration interaction study

Theresa Lynn Windus
Iowa State University, twindus@iastate.edu

Daniel Theis
Iowa State University

Joseph Ivanic
Frederick National Laboratory for Cancer Research

Klaus Ruedenberg
Iowa State University

The transition from the open minimum to the ring minimum on the ground state and on the lowest excited state of like symmetry in ozone: A configuration interaction study

Abstract
The metastable ring structure of the ozone 11A1 ground state, which theoretical calculations have shown to exist, has so far eluded experimental detection. An accurate prediction for the energy difference between this isomer and the lower open structure is therefore of interest, as is a prediction for the isomerization barrier between them, which results from interactions between the lowest two 1A1 states. In the present work, valence correlated energies of the 11A1 state and the 21A1 state were calculated at the 11A1 open minimum, the 11A1 ring minimum, the transition state between these two minima, the minimum of the 21A1 state, and the conical intersection between the two states. The geometries were determined at the full-valence multi-configuration self-consistent-field level. Configuration interaction (CI) expansions up to quadruple excitations were calculated with triple-zeta atomic basis sets. The CI expansions based on eight different reference configuration spaces were explored. To obtain some of the quadruple excitation energies, the method of Correlation Energy Extrapolation by Intrinsic Scaling was generalized to the simultaneous extrapolation for two states. This extrapolation method was shown to be very accurate. On the other hand, none of the CI expansions were found to have converged to millihartree (mh) accuracy at the quadruple excitation level. The data suggest that *convergence* to mh accuracy is probably attained at the sextuple excitation level. On the 11A1 state, the present calculations yield the estimates of (ring minimum—open minimum) ~45–50 mh and (transition state—open minimum) ~85–90 mh. For the (21A1–1A1) excitation energy, the estimate of ~130–170 mh is found at the open minimum and 270–310 mh at the ring minimum. At the transition state, the difference (21A1–1A1) is found to be between 1 and 10 mh. The geometry of the transition state on the 11A1 surface and that of the minimum on the 21A1 surface nearly coincide. More accurate predictions of the energy*differences* also require CI expansions to at least sextuple excitations with respect to the valence space. For every wave function considered, the omission of the correlations of the 2s oxygen orbitals, which is a widely used approximation, was found to cause errors of about ±10 mh with respect to theenergy differences.

Keywords
Wave functions, Rings, Ozone, Potential energy surfaces, exitation energies

Disciplines
Biological and Chemical Physics | Chemistry

Comments
This article is published as Theis, Daniel, Joseph Ivanic, Theresa L. Windus, and Klaus Ruedenberg. "The transition from the open minimum to the ring minimum on the ground state and on the lowest excited state of like symmetry in ozone: A configuration interaction study." The Journal of chemical physics 144, no. 10 (2016): 104304. 10.1063/1.4942019. Posted with permission.

The transition from the open minimum to the ring minimum on the ground state and on the lowest excited state of like symmetry in ozone: A configuration interaction study

Daniel Theis, Joseph Ivanic, Theresa L. Windus, and Klaus Ruedenberg

Citation: The Journal of Chemical Physics **144**, 104304 (2016);
View online: https://doi.org/10.1063/1.4942019
View Table of Contents: http://aip.scitation.org/toc/jcp/144/10
Published by the American Institute of Physics

The transition from the open minimum to the ring minimum on the ground state and on the lowest excited state of like symmetry in ozone: A configuration interaction study

Daniel Theis,[1] Joseph Ivanic,[2] Theresa L. Windus,[1] and Klaus Ruedenberg[1]
[1]*Department of Chemistry and Ames Laboratory USDOE, Iowa State University, Ames, Iowa 50011, USA*
[2]*Advanced Biomedical Computing Center, Frederick National Laboratory for Cancer Research, DSITP, Leidos Biomedical Research, Inc., Frederick, Maryland 21702, USA*

(Received 17 November 2015; accepted 26 January 2016; published online 10 March 2016)

The metastable ring structure of the ozone 1^1A_1 ground state, which theoretical calculations have shown to exist, has so far eluded experimental detection. An accurate prediction for the energy difference between this isomer and the lower open structure is therefore of interest, as is a prediction for the isomerization barrier between them, which results from interactions between the lowest two $^1A_1$ states. In the present work, valence correlated energies of the 1^1A_1 state and the 2^1A_1 state were calculated at the 1^1A_1 open minimum, the 1^1A_1 ring minimum, the transition state between these two minima, the minimum of the 2^1A_1 state, and the conical intersection between the two states. The geometries were determined at the full-valence multi-configuration self-consistent-field level. Configuration interaction (CI) expansions up to quadruple excitations were calculated with triple-zeta atomic basis sets. The CI expansions based on eight different reference configuration spaces were explored. To obtain some of the quadruple excitation energies, the method of Correlation Energy Extrapolation by Intrinsic Scaling was generalized to the simultaneous extrapolation for two states. This extrapolation method was shown to be very accurate. On the other hand, none of the CI expansions were found to have converged to millihartree (mh) accuracy at the quadruple excitation level. The data suggest that *convergence* to mh accuracy is probably attained at the sextuple excitation level. On the 1^1A_1 state, the present calculations yield the estimates of (ring minimum—open minimum) ~45–50 mh and (transition state—open minimum) ~85–90 mh. For the (2^1A_1–$^1A_1$) excitation energy, the estimate of ~130–170 mh is found at the open minimum and 270–310 mh at the ring minimum. At the transition state, the difference (2^1A_1–$^1A_1$) is found to be between 1 and 10 mh. The geometry of the transition state on the 1^1A_1 surface and that of the minimum on the 2^1A_1 surface nearly coincide. More accurate predictions of the energy *differences* also require CI expansions to at least sextuple excitations with respect to the valence space. For every wave function considered, the omission of the correlations of the 2s oxygen orbitals, which is a widely used approximation, was found to cause errors of about ±10 mh with respect to the energy differences. [http://dx.doi.org/10.1063/1.4942019]

NOMENCLATURE

CASSCF	Complete active space self-consistent field
FORS	Full optimized reaction space
CEEIS	Correlation energy extrapolation by intrinsic scaling
SD	Single plus double excitations
SDT	Single plus double plus triple excitations
SDTQ	Single plus double plus triple plus quadruple excitations
CISD	configuration interaction for SD
CISDT	configuration interaction for SDT
CISDTQ	configuration interaction for SDTQ
MRCISD	CISD with respect to a multi-determinant-reference
MRCISDT	CISDT with respect to a multi-determinant-reference
MRCISDTQ	CISDQ with respect to a multi-determinant-reference
VSDNO	Natural orbitals in the virtual space of a MRCISD calculation

I. INTRODUCTION

The ozone molecule is important in many respects. Its ultraviolet absorption in the stratosphere is beneficial[1] while its presence in the lower atmosphere is harmful.[2] Its strong oxidative power has made it a heavily used sterilization agent in industry[3] and a key oxidizing agent in chemical research laboratories.[4] A wide range of experimental and theoretical studies have been made on this fundamental molecule.

Diverse spectroscopic observations have yielded significant amounts of experimental information regarding the excited states. Numerous theoretical studies have been

performed to address the challenges presented by the excited state potential energy surfaces (PESs). Of particular interest is the potential existence of metastable excited state minima.[5] Most high accuracy spectroscopic measurements have only been able to infer the existence of such minima.[6] But metastable excited minima were identified from anion photoelectron spectroscopic measurements,[7] and these minima were reproduced by accurate theoretical calculations.[8–11]

A significant amount of work has also been performed to elucidate the photodissociation[12] of ozone because of its important role in the ozone-oxygen cycle.[13,14] The wavelength dependences of the quantum yields and branching ratios have been determined by dynamics calculations that are based on adiabatic potential energy surfaces that were specifically calculated for these problems[15,16] and on coupling potential terms for non-adiabatic interactions.[17]

Another set of issues is associated with the ground state. Its vibrational spectrum presents a challenge in as much as it cannot be accurately recovered by uncorrelated wave functions. Therefore, the reproduction of this spectrum has been used to test the performance of wave functions that include correlation in various ways[9–11,18] and, on the other hand, to assess multi-reference diagnostics.[19] For a considerable time, the bonding structure of ozone was a subject of debate, viz., whether the accurate electronic wave function of the ground state implies a conceptual interpretation as a diradical[20] or a genuine closed shell singlet.[9] A thorough *ab initio* investigation[21] of a series of triatomic molecules containing oxygen and sulfur has clarified the various degrees of partial radical character of ozone and its analogues. The description of the ground state dissociation path and the recovery of the experimental dissociation energy have proven particularly challenging and required extremely accurate wave functions.[22–24]

Conversely, the theoretical approach has revealed certain features of the ground state potential energy surface that have posed a great challenge to experimentalists. Many high level *ab initio* calculations have established beyond any doubt that there exists a metastable ring structure of ozone with D_{3h} symmetry. But this isomer has so far eluded experimental detection even though interest in the ozone ring is over 100 years old.[25] The first quantitative *ab initio* predictions of a closed ozone conformer were made in the early 1970s by Hay and Goddard and, then, by other authors.[26] Extremely accurate calculations were made by Lee[27] and by Qu, Zhu, and Schinke,[28] where references to further previous work are given. The first to explore the barrier that separates the ozone ring conformer from the open conformer were Xantheas, Atchity, Elbert, and Ruedenberg.[29,30] Their extensive and thorough *ab initio* investigations (based on multi-configuration-self-consistent-field calculations in the full valence space—FORS-CASSCF) showed that the ring isomer is surrounded by a substantial ridge in C_s symmetry on which three saddle points, each in C_{2v} symmetry, provide the transition states between the ring minimum and the three open minima on the potential energy surface. Their investigations demonstrated that the ridge is the result of an avoided crossing between the $^1A'$ ground state and the lowest excited $^1A'$ state and, notably, that the two states in fact touch each other along a closed conical intersection seam in C_s symmetry.[29,30] This intersection seam crosses the three C_{2v} symmetry planes in conical intersection points that lie near the three transition states.[29] Furthermore, the excited $^1A'$ state was shown to have three minima that lie extremely close to the transition states of the ground state.[29] Analogous features were found by Ivanic, Atchity, and Ruedenberg[31] on the potential energy surfaces of the ozone homologues S_3, S_2O, and SO_2.

On the basis of theoretical calculations, Fleming, Wolczanski, and Hoffman suggested that the closed conformer of ozone, as well as its sulfur analogue, might be trapped in transition metal complexes.[32] Qu, Zhu, and Schinke reviewed various proposals that have been made for accessing the elusive ring isomer.[28] These authors suggested that possible mechanisms might be photochemical excitations followed by radiationless reaction paths that pass through the conical intersection seam. This conjecture motivated DeVico *et al.* to revisit the structure of the two potential energy surfaces in the region of the transition state of the ground state and the conical intersection.[33]

Since general experience has shown the ozone PES to be very sensitive to dynamic correlation,[22] DeVico *et al.* examined this region by means of wave functions that account for more electron correlation than was included in the calculations of Refs. 29 and 30. The calculations of DeVico *et al.* were based on several versions of multi-configurational second-order complete-active-space perturbation theory (MS-CASPT2). Special care had to be taken to avoid erratic behavior of the energy along the reaction path in the transition state region.

In the present study, the transition from the open minimum to the ring minimum is examined by means of wave functions that include correlation contributions up to quadruple excitations beyond multi-configurational reference states. To this end, MRCISDTQ wave functions for the two lowest singlet states are determined. To recover the correlation contributions, the Correlation Energy Extrapolation by Intrinsic Scaling (CEEIS) is used.[34] Since the determination of the wave functions in the region of interest requires the state averaged approach, the generalization of the CEEIS method to the simultaneous treatment of several states, which was first used by Bytautas for the B_2 molecule,[35] is further developed and generalized to polyatomic molecules. An important aspect of the present work is to determine whether, for a multi-state application in a polyatomic molecule with substantial correlation interactions, the CEEIS extrapolation methodology retains the same high convergence quality that it exhibits when applied to diatomic molecules.[36]

II. THE CEEIS METHOD FOR MULTIPLE STATES

This section contains a brief summary of the CEEIS method. The basis of the CEEIS procedure is an exact expansion of the full configuration interaction (CI) energy, E_k^{FCI}, of each state as a sum of energy contributions of the various configurational excitation levels,

$$E_k^{FCI} = E_k(0) + \Delta E_k(1,2) + \sum_{x \geq 3} \Delta E_k(x), \qquad (2.1)$$

where the subscript k specifies the electronic state and the excitation levels are indicated in the parentheses. The term $E_k(0)$ denotes the reference energy. The term $\Delta E_k(1,2) = E_k(2) - E_k(0)$ denotes the combined incremental energy contribution due to the inclusion of single and double excitations levels beyond the reference function. The sum over x covers all excitation levels above the double excitations. The term $\Delta E_k(x)$ denotes the incremental energy contribution that is due to the *addition of* excitation level x,

$$\Delta E_k(x) = E_k(x) - E_k(x-1). \tag{2.2}$$

In the CEEIS method, values for the incremental energy contributions of every excitation above $x = 3$ are extrapolated from the incremental energy contributions that were determined for the single, double, and triple excitations. These extrapolations are based on calculating, at each excitation level x, approximations $\Delta E_k(x|m)$, which are obtained by including only the excitations generated by up to a number m of active virtual orbitals, where $m < M$ = the *total* number of virtual orbitals (the virtual orbital space being the part of the basis orbital space that is unoccupied in the reference function). It was shown in previous papers[35] that the convergences of $\Delta E_k(x|m)$ with increasing m to the limit $\Delta E_k(x|M)$ *at different excitation levels* x are linearly related. Specifically, as the number of active virtual orbitals, m, is increased, the change that occurs for $\Delta E_k(x|m)$ is linearly proportional to the change that occurs for $\Delta E_k(x*|m)$, where $x*$ is a lower excitation level than x. This linear proportionality is expressed by the equation

$$\Delta E_k(x|m) = a_{k,x}\Delta E_k(x*|m) + c_{k,x}. \tag{2.3}$$

Thus, if $\Delta E_k(x*) = \Delta E_k(x*|M)$ is known, the value of $\Delta E_k(x) = \Delta E_k(x|M)$ is obtained as follows. Step 1: Values for $\Delta E_k(x|m)$ and $\Delta E_k(x*|m)$ are calculated for a range of m values that are considerably smaller than M. Step 2: These values of $\Delta E_k(x|m)$ and $\Delta E_k(x*|m)$ are used in a least-mean-squares fit to determine the coefficients $a_{k,x}$ and $c_{k,x}$ in Eq. (2.3). Step 3: The values of $a_{k,x}$ and $c_{k,x}$ and the known value of $\Delta E_k(x*) = \Delta E_k(x*|M)$ are used to extrapolate to the value of $\Delta E_k(x) = \Delta E_k(x|M)$. For $\Delta E_k(1,2)$, the exact value is calculated. When possible the exact value is also calculated for $\Delta E_k(3)$. If the exact calculation of $\Delta E_k(3)$ is not affordable, its value is extrapolated from $\Delta E_k(1,2)$ in a similar manner. For all excitation levels $x \geq 4$, extrapolations using $x* = x - 2$ typically require lower values for m than the values that are needed for the extrapolation using $x* = x - 1$. Hence, for $x > 4$, $\Delta E_k(x)$ is extrapolated using $\Delta E_k(x-2)$. However, for $\Delta E_k(4)$, a more reliable estimate is obtained by using $\Delta E_k(1,2)$ rather than only $\Delta E_k(2)$ for $\Delta E_k(x^*)$.

Various kinds of reference functions will be considered, which are obtained as follows. A preliminary state-averaged CAS MCSCF (complete-active-space multi-configuration-self-consistent-field) calculation is performed in the full valence space in order to identify the dominant electronic configurations for each state. On this basis, more affordable CAS subspaces are then identified that have smaller numbers of determinants while still generating the dominant configurations of every state of interest. Reduced reference functions are then obtained by new state-averaged CAS MCSCF calculation in such subspaces.

Once the occupied orbitals have been optimized, a preliminary MRCISD (multi-determinant-reference singles + doubles configuration interaction) calculation is performed to determine energies and one-particle density matrices for each of the states of interest. The one-particle density matrices are then used to form a state-averaged one-particle density matrix. The virtual-virtual block of this state averaged one-particle density matrix is diagonalized to obtain state-averaged natural orbitals for the virtual orbital space (VSDNOs). The VSDNOs, ordered according to decreasing occupation numbers, provide the basis for calculating the CI energies that are needed for the CEEIS extrapolation of each state's energy.

Once these preliminary calculations are complete, CI calculations are performed at multiple excitation levels x and using varying numbers m of VSDNOs in order to evaluate all $\Delta E_k(x|m)$ that are needed for the CEEIS of each electronic state. Once all $\Delta E_k(x|m)$ have been determined, *separate CEEIS extrapolations are performed for each electronic state of interest*. An automated procedure has been developed for the CEEIS method running through all states of interest. It is included in the GAMESS[37] molecular program suite.

The range of the m values to be used for the extrapolations to the CEEIS energies has to be chosen by the user, even if the automated procedure is used. Typically, it is advisable to choose the lowest value for m not to lie significantly below the total number of virtual orbitals that are generated by a double zeta basis set. Below that number of virtual orbitals, the changes in $\Delta E_k(x|m)$ and $\Delta E_k(x*|m)$ may not be linearly proportional. It is important to examine the plots of the values of $\Delta E_k(x|m)$ against the values of $\Delta E_k(x*|m)$ to ascertain that the changes in $\Delta E_k(x|m)$ and $\Delta E_k(x*|m)$ are indeed linearly proportional for the chosen values of m.

Furthermore, when selecting the energies that are used to determine the $\Delta E_k(x|m)$ values for the extrapolation, special precaution is required when two or more electronic states are nearly degenerate. A careful analysis of the dominant configurations of each state's wave function must be performed to ensure that the energy differences that are used in the extrapolations are associated with the same reference wave function (i.e., have the same dominant electronic configurations). This is necessary because the *order* of the energies of near degenerate states may change as the number of active virtual orbitals is increased or as the maximum excitation level of the calculation is changed.

III. FULL VALENCE SPACE POTENTIAL ENERGY SURFACES OF THE 1^1A_1 AND 2^1A_1 STATES OF OZONE

The full-valence space of ozone consists of 12 orbitals and 18 electrons. State-averaged CASSCF(18,12) calculations were performed using Dunning's *cc-p*VTZ and *cc-p*VQZ basis sets.[38] Optimizations were performed to determine the following five geometries:

OM = the open minimum of the 1^1A_1 state,

RM = the ring minimum of the 1^1A_1 state,

TS = the transition state that separates these minima on the 1^1A_1 surface,

XM = the minimum of the 2^1A_1, and

CI = the conical intersection between the two states.

In the subsequent text and tables, the abbreviations OM, RM, TS, XM, and CI will continue to be used to denote these five geometries.

Table I shows the optimized geometries and the energies of each state at these geometries *relative to the respective energies of the open minimum of the* 1^1A_1 *state*. The absolute energies for the two basis sets at the OM geometries are given in footnotes *d* and *e* of Table I. The data show that the geometries obtained using the *cc-p*VTZ and *cc-p*VQZ basis sets differ from each other by less than 0.004 Å and 0.1° and that their relative energies differ by less than 2 mh. These results justify the use of the more affordable *cc-p*VTZ basis set.

The theoretical geometries of the open minimum (first row of Table I) can be compared to the experimental data[39] listed in footnote *b* of that table. The deviations of the bond lengths are 0.014 Å and 0.010 Å for the *cc-p*VTZ and *cc-p*VQZ basis set calculations, respectively. The corresponding bond angle deviations are 0.3° and 0.2°. The slightly deteriorating effect of state-averaging is exhibited by comparing these deviations with those that are found by the *state-specific* calculations, which are listed in footnote *c* of Table I. The state-specific CASSCF(18,12)/*cc-p*VTZ and /*cc-p*VQZ calculations yield deviations from the experiment of 0.007 Å and 0.003 Å for the bond length, and 0.1° and 0.0° for the bond angle, respectively.

In Secs. IV–VIII, all correlation energy calculations are performed at the optimized state-averaged CASSCF(18,12)/*cc-p*VQZ geometries.

The conical intersection point was determined with the *cc-p*VQZ basis. Figure 1 displays contour plots of the potential energy surfaces for the 1^1A_1 and 2^1A_1 states (panels (a) and (b), respectively) and for the energy difference between these states (panel (c)) in the region near the conical intersection. The region that is shown in panel (c) is indicated by the green box in panels (a) and (b) and is expressed in terms of coordinates q and p, the reaction coordinate and the normal mode that is perpendicular to the reaction coordinate, respectively. The contours show that the position of the minimum of the 2^1A_1 state is nearly identical to the position of the 1^1A_1 transition state. For the 1^1A_1 state, the rate of descent towards the open minimum (the lower right) is larger than the rate of descent towards the ring minimum (the upper left). In contrast, the potential energy surface of the 2^1A_1 state has a rate of ascent in the direction of the 1^1A_1 open minimum that is smaller than its rate of ascent towards the 1^1A_1 ring minimum. This behavior is consistent with the changes that are observed in potential energy surfaces of nonadiabatically coupled states near a conical intersection or avoided crossing. It is a consequence of the switch in the dominant diabatic states. The data in Table I show that, at the conical intersection geometry, the energy gap between the two states is less than 0.005 mh for the *cc-p*VQZ basis and 0.25 mh for the *cc-p*VTZ basis.

IV. CONFIGURATION INTERACTION CALCULATIONS

A. Analysis of the full valence space structure

Since the generation of the dynamic correlation by excitations from the full CAS(18,12) reference space exceeded the available computational resources, the suitability of smaller reference spaces had to be explored. Such spaces must account for the changes in the *dominant* configurations of the 1^1A_1 and 2^1A_1 states as the geometry of O_3 changes from the open minimum to the ring minimum. To this end, a close examination of the configurational structures of the two states in the *full* valence space is instructive. Figure 2 displays the 12 canonicalized orbitals obtained from the state-averaged CASSCF(18,12)/*cc-p*VTZ calculations at the open and ring minima. Between the orbitals of each pair, the orbital label (in C_{2v} symmetry) is given. Under each orbital contour, the occupation in both the 1^1A_1 state and the 2^1A_1 state as well as its canonicalized orbital energy is listed.

TABLE I. Optimized CASSCF(18,12) geometries and 1^1A_1 and 2^1A_1 state energies of several points along the 1^1A_1 and 2^1A_1 potential energy surfaces, calculated using the *cc-p*VTZ and *cc-p*VQZ basis sets. (Bond lengths and bond angles are given in Å and degrees, respectively. Energies (E) are reported in mh relative to their respective energies at the 1^1A_1 state open minimum.)

	*cc-p*VTZ Basis set				*cc-p*VQZ Basis set			
Geometry[a]	E(1^1A_1)	E(2^1A_1)	R_{OO}	∠	E(1^1A_1)	E(2^1A_1)	R_{OO}	∠
OM[b,c]	0.00[d]	150.96	1.292	116.5	0.00[e]	152.55	1.288	116.6
RM	47.60	335.13	1.466	60.0	48.86	337.98	1.465	59.9
TS	84.13	84.78	1.424	84.1	85.12	85.96	1.428	84.0
XM	83.42	84.68	1.431	83.8	84.96	85.57	1.428	83.8
CI	87.36	87.61	1.491	83.3	88.85	88.85	1.491	83.3

[a]The following abbreviations are used in this and the following tables: OM = 1^1A_1 state open minimum, RM = 1^1A_1 state ring minimum, TS = 1^1A_1 state transition state, XM = 2^1A_1 state minimum, CI = conical intersection between the 1^1A_1 state and the 2^1A_1 state.

[b]The experimental values of OM for R_{OO} and ∠ are 1.278 Å and 116.8°, respectively.[39]

[c]The bond lengths and bond angles that are listed for each geometry were determined from state-averaged CASSCF(18,12) calculations. Single-state CASSCF(18,12) calculations for the 1^1A_1 state for the optimized open minimum geometry yielded R_{OO} = 1.285 Å and ∠ = 116.7° for the *cc-p*VTZ basis set and R_{OO} = 1.281 Å and ∠ = 116.8° for the *cc-p*VQZ basis set.

[d]The absolute *cc-p*VTZ energy for this geometry is −224.569 832 hartree.

[e]The absolute *cc-p*VQZ energy for this geometry is −224.586 929 hartree.

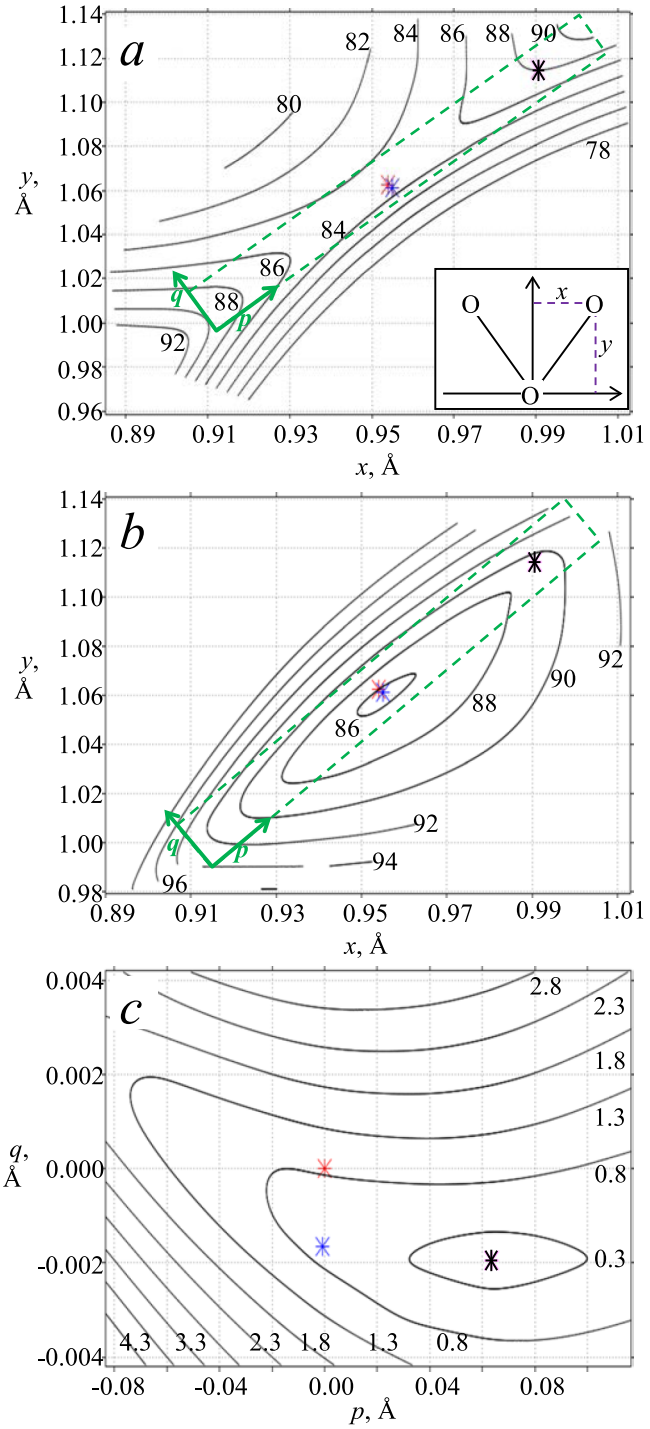

FIG. 1. Contour plots near the conical intersection: (a) the 1^1A_1 state potential energy surface; (b) the 2^1A_1 state potential energy surface; (c) the energy difference $E(2^1A_1) - E(1^1A_1)$. The energies were obtained from state-averaged CASSCF(18,12)/*cc-p*VQZ calculations and are given in mh. In panels (a) and (b), the energies given for the contours are with respect to the energy of the 1^1A_1 state at the open minimum. The coordinates p and q of panel (c) are indicated in panels (a) and (b) by green vectors. The range of panel (c) is indicated in (a) and (b) by the dashed green boxes. Note the difference in the scales of the coordinates and the energies. The red, blue, and black asterisk-like symbols identify the positions of the TS, the XM, and the CI, respectively.

The dominant parts of the wave functions for each state (i.e., the normalized, spin-adapted determinants with coefficients ≥0.1 in magnitude) are displayed in Tables II and III. Table II lists the expansions of the dominant parts of the wave functions in terms of normalized, spin-adapted determinants at each of the discussed geometries. Table III lists the orbital occupations of the 12 determinants that occur in Table II. The results documented in these tables show that the determinants $|D_1\rangle$, $|D_2\rangle$, $|D_3\rangle$, and $|D_4\rangle$, which are indicated by bold faced font in Tables II and III, are the most important determinants for the generation of both states at all of the geometries, with determinants $|D_1\rangle$ and $|D_2\rangle$ usually making contributions that are slightly larger than the contributions from $|D_3\rangle$ and $|D_4\rangle$. Additionally, the last column in Table III shows that all of the determinants listed in Table III, including $|D_3\rangle$ and $|D_4\rangle$, can be generated by single and double excitations from $|D_1\rangle$ or $|D_2\rangle$.

The active orbitals that distinguish $|D_1\rangle$ and $|D_2\rangle$ are the orbitals $4b_1$ and $2b_2$. They are indicated by symbols in red font in Figure 2. For the determinants $|D_3\rangle$ and $|D_4\rangle$, these orbitals remain doubly occupied. Instead, the determinants $|D_3\rangle$ and $|D_4\rangle$ differ in the occupancies of orbitals $6a_1$ and $1a_2$, which are indicated by symbols in blue font in Figure 2. In Table III, these four orbitals $4b_1$, $2b_2$, $6a_1$ and $1a_2$ are all indicated by bold faced font. The determinants $|D_1\rangle$ and $|D_2\rangle$ span the full CAS(2,2) subspace of $^1A_1$ symmetry that is generated by the active orbitals $4b_1$ and $2b_2$. Similarly, the determinants $|D_1\rangle$, $|D_2\rangle$, $|D_3\rangle$, and $|D_4\rangle$ span the full CAS(6,4) subspace of $^1A_1$ symmetry that is generated by the active orbitals $6a_1$, $1a_2$, $4b_1$, and $2b_2$.

In all the dominant determinants listed in Tables II and III, the valence orbitals $3a_1$, $4a_1$, and $2b_1$ remain doubly occupied, and they are therefore not included in Table III. Figure 2 shows that, in fact, they have occupations nearly equal to 2 in the *full* CAS(18,12) wave functions for *both* states. From the images that are displayed for these orbitals in Figure 2, it is apparent that they are dominated by the 2s atomic orbitals on the three oxygen atoms. Based on that fact, the set of the orbitals $3a_1$, $4a_1$, and $2b_1$ will be referred to as the "2*s* group" in the subsequent discussion.

On the other hand, Table III shows that orbitals $5b_1$ and $7a_1$ are unoccupied in the determinants $|D_1\rangle$, $|D_2\rangle$, $|D_3\rangle$, and $|D_4\rangle$, and it is apparent from Figure 2 that these two orbitals have *very* low occupations in the *full* CAS(18,12) wave functions for *both* states. For this reason, these two orbitals will be referred as the "weak group" in the subsequent discussion.

B. Reduced reference-active and correlation-active spaces

In view of the preceding analysis, the following restrictions of the full CAS(18,12) valence space seem reasonable strategies for achieving reductions in the number of correlating excited configurations:

- Move the "weak MO group" ($7a_1$, $5b_1$) from the active space into the virtual space.
- Move the "2s-MO group" ($3a_1$, $4a_1$, $2b_1$), which are indicated by green font in Figure 2, from the active space to the inactive occupied space.
- Limit the reference space to the full space generated by the "strong correlation group" of the orbitals $4b_1$, $2b_2$, $6a_1$, $1a_2$.

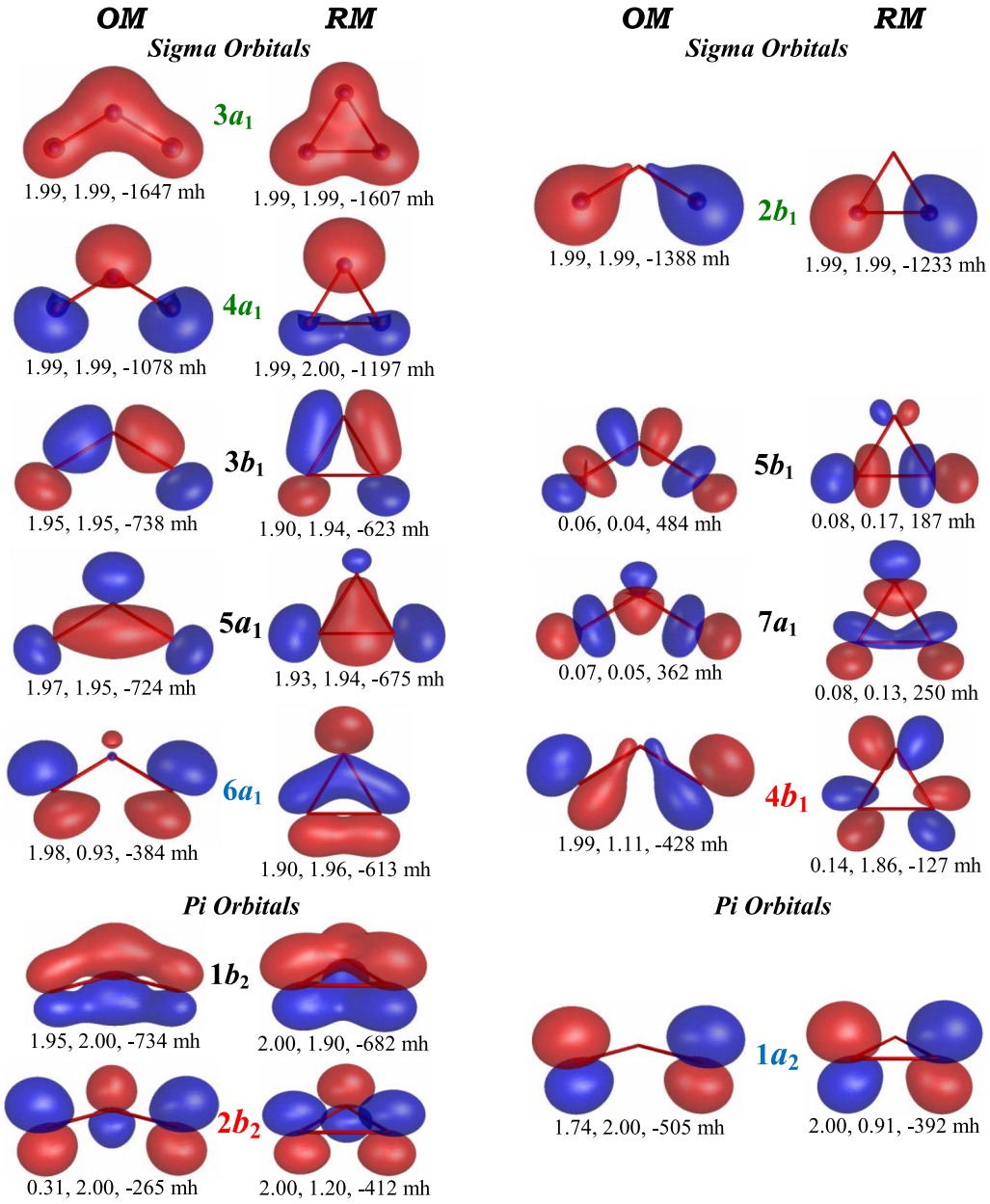

FIG. 2. Canonical valence orbitals of the state-averaged CASSCF(18,12)/*cc-p*VTZ wave functions for the 1^1A_1 and 2^1A_1 states of O_3 at the OM and RM. Between the orbitals of each pair, the symmetry label (in C_{2v}) is given. Below each orbital, the orbital occupations in the 1^1A_1 state and in the 2^1A_1 state, as well as the canonical orbital energy are listed, in that order.

• Limit the reference space to the full space generated by the "minimal reaction group" of the orbitals $4b_1$, $2b_2$.

In light of these criteria, several combinations of reference and excitation spaces were considered in forming wave functions. They differ with respect to the valence orbitals that are *active in the reference space* and those that are *correlation-active*, i.e., subject to excitations into virtual orbitals. Tables IV and V give the specifications of these wave functions in the ORMAS (occupation restricted multiple active space[40]) format, which was used in the calculation. Table IV contains four wave functions, in which *the* "2*s-group*" *is correlation-active*. Table V contains four wave functions, in which *the* "2*s-group*" *is correlation-inactive*, which is a popular assumption. Each table consists of four subtables, each of which describes a wave function. It is identified by the symbol heading in the first column of the subtable. The headings of columns 2, 3, 4, and 5 of each wave function subtable specify, respectively, the following:

• those orbitals that are reference-inactive as well as correlation-inactive;

• those orbitals that are reference-inactive but correlation-active;

• those orbitals that are reference-active as well as correlation-active; and

• the virtual orbitals that are used for this wave function, as indicated by the overall column headings below the table title. The four numerical rows of each subtable contain the actual information regarding the electron occupations. These rows correspond to the reference space, the reference space + SD excitations, and similarly to adding SDT and SDTQ excitations, as indicated by the abbreviations in the first column of the rows. The numbers in these rows give the

TABLE II. Expressions for the dominant parts of the CASSCF(18,12)/*cc–p*VTZ wave functions for the 1^1A_1 and 2^1A_1 states of O_3 in terms of spin-adapted determinants.[a]

Geometry	Dominant configurations of the wave functions[b,c]
OM	$\|1^1A_1\rangle \approx 0.8922\|\boldsymbol{D_1}\rangle - 0.3290\|\boldsymbol{D_3}\rangle$
	$\|2^1A_1\rangle \approx 0.7253\|\boldsymbol{D_4}\rangle - 0.6468\|\boldsymbol{D_2}\rangle$
RM	$\|1^1A_1\rangle \approx 0.9259\|\boldsymbol{D_2}\rangle - 0.1301\|\boldsymbol{D_4}\rangle - 0.1009\|D_5\rangle$
	$\|2^1A_1\rangle \approx 0.6692\|\boldsymbol{D_3}\rangle - 0.5981\|\boldsymbol{D_1}\rangle - 0.1116\|D_6\rangle$
TS	$\|1^1A_1\rangle \approx 0.8617\|\boldsymbol{D_2}\rangle - 0.3798\|\boldsymbol{D_4}\rangle - 0.1079\|\boldsymbol{D_1}\rangle - 0.1075\|D_7\rangle$
	$\|2^1A_1\rangle \approx 0.7722\|\boldsymbol{D_1}\rangle - 0.5171\|\boldsymbol{D_3}\rangle$
XM	$\|1^1A_1\rangle \approx 0.7225\|\boldsymbol{D_1}\rangle - 0.4558\|\boldsymbol{D_3}\rangle - 0.2298\|D_8\rangle - 0.1882\|\boldsymbol{D_2}\rangle$
	$\|2^1A_1\rangle \approx 0.7791\|\boldsymbol{D_2}\rangle - 0.2805\|\boldsymbol{D_4}\rangle - 0.2510\|D_9\rangle + 0.1962\|D_{10}\rangle$
	$+0.1723\|D_{11}\rangle + 0.1560\|\boldsymbol{D_1}\rangle + 0.1506\|D_{12}\rangle - 0.1342\|\boldsymbol{D_3}\rangle$
CI	$\|1^1A_1\rangle \approx 0.7560\|\boldsymbol{D_1}\rangle - 0.5340\|\boldsymbol{D_3}\rangle$
	$\|2^1A_1\rangle \approx 0.8479\|\boldsymbol{D_2}\rangle - 0.4024\|\boldsymbol{D_4}\rangle - 0.1180\|D_7\rangle - 0.1018\|D_5\rangle$

[a]Listed are the normalized $^1A_1$ spin-adapted determinants, $|D_j\rangle$, that have coefficients with magnitudes greater than or equal to 0.1.
[b]Bold font indicates the two $^1A_1$ spin-adapted determinants, $|D_1\rangle$ and $|D_2\rangle$, which constitute the CAS(2,2).
[c]Bold font also indicates the two additional $^1A_1$ spin-adapted determinants, $|D_3\rangle$ and $|D_4\rangle$, that along with $|D_1\rangle$ and $|D_2\rangle$ constitute the CAS(6,4).

minimum number and the maximum number of electrons that can occupy the (reference or virtual) orbitals that are specified in the header of each column.

Table IV lists the specifications for four wave functions, in which the "2s-group" is correlation-active, although not necessarily reference-active. They are as follows:

• CAS(18,12): This is the full valence space wave function with the corresponding virtual space of 75 orbitals.

• CAS(18,10): This space is obtained by moving the "weak MO group" (orbitals $7a_1$, $5b_1$) from the preceding full valence space into the virtual space, which now has 77 orbitals. The reference space is thus reduced. But all remaining valence orbitals are still active in the reference space and with respect to SD, SDT, and SDTQ excitations into the virtual space.

• CAS(6,4): Only the orbitals $4b_1$, $2b_2$, $6a_1$, $1a_2$ of the "strong correlation group" are active in the reference function. But *all* valence orbitals are correlation-active. Moreover, the reference-inactive orbitals can also be excited into the reference-active orbitals by SD-excitations. However, the weak MO group is placed into the virtual space, as in the CAS(18,10) case.

• CAS(2,2): Only the orbitals $4b_1$, $2b_2$ of the "minimal reaction group" are active in the reference function. But *all* valence orbitals are correlation active. The reference-inactive

TABLE III. Orbital occupations of the dominant spin-adapted determinants of the CASSCF(18,12)/*cc–pV*TZ wave functions for the 1^1A_1 and 2^1A_1 states of O_3.[a]

Spin adapted determinant[b,c]	Active orbitals[d,e,f,g,h]									Excitation with respect to $\|\boldsymbol{D_1}\rangle$ or $\|\boldsymbol{D_2}\rangle$
	$5a_1$	$3b_1$	$1b_2$	$\boldsymbol{6a_1}$	$\boldsymbol{1a_2}$	$\boldsymbol{4b_1}$	$\boldsymbol{2b_2}$	$7a_1$	$5b_1$	
$\|\boldsymbol{D_1}\rangle$	2	2	2	**2**	**2**	**2**				…
$\|\boldsymbol{D_2}\rangle$	2	2	2	**2**	**2**		**2**			…
$\|\boldsymbol{D_3}\rangle$	2	2	2	**2**		**2**	**2**			$\|\boldsymbol{D_1}, (\boldsymbol{1a_2})^2 \rightarrow (\boldsymbol{2b_2})^2\rangle$
$\|\boldsymbol{D_4}\rangle$	2	2	2		**2**	**2**	**2**			$\|\boldsymbol{D_2}, (\boldsymbol{6a_1})^2 \rightarrow (\boldsymbol{4b_1})^2\rangle$
$\|D_5\rangle$		2	2	**2**	**2**		**2**	2		$\|\boldsymbol{D_2}, (5a_1)^2 \rightarrow (7a_1)^2\rangle$
$\|D_6\rangle$	2	2	2	**2**			**2**		2	$\|\boldsymbol{D_2}, (\boldsymbol{1a_2})^2 \rightarrow (5b_1)^2\rangle$
$\|D_7\rangle$	2		2	**2**	**2**		**2**		2	$\|\boldsymbol{D_2}, (3b_1)^2 \rightarrow (5b_1)^2\rangle$
$\|D_8\rangle$	2	2	1	**2**	**2**	**2**	**1**			$\|\boldsymbol{D_1}, (1b_2)^2 \rightarrow (1b_2)^1(\boldsymbol{2b_2})^1\rangle$
$\|D_9\rangle$	2	1	2	**2**	**2**		**2**		1	$\|\boldsymbol{D_2}, (3b_1)^2 \rightarrow (3b_1)^1(5b_1)^1\rangle$
$\|D_{10}\rangle$	1	2	2	**1**	**2**	**2**	**2**			$\|\boldsymbol{D_1}, (5a_1)^2(\boldsymbol{6a_1})^2 \rightarrow (5a_1)^1(\boldsymbol{6a_1})^1(\boldsymbol{2b_2})^2\rangle$
$\|D_{11}\rangle$	1	2	2	**2**	**2**		**2**	1		$\|\boldsymbol{D_2}, (5a_1)^2 \rightarrow (5a_1)^1(7a_1)^1\rangle$
$\|D_{12}\rangle$	2	2	2	**1**	**2**		**2**	1		$\|\boldsymbol{D_2}, (\boldsymbol{6a_1})^2 \rightarrow (\boldsymbol{6a_1})^1(7a_1)^1\rangle$

[a]Listed are the orbital occupations of the $^1A_1$ spin-adapted determinants that occur in Table II. The spin-adapted determinants with singly occupied orbitals are normalized combinations of two Slater-determinants.
[b]Indicated in bold font are the configurations, $|D_1\rangle$ and $|D_2\rangle$, that span the $^1A_1$ subspace of the CAS(2,2).
[c]Also indicated in bold are the configurations, $|D_3\rangle$ and $|D_4\rangle$, that, together with shaded $|D_1\rangle$ and $|D_2\rangle$, span the $^1A_1$ subspace of the CAS(6,4).
[d]The doubly occupied core orbitals $1a_1$, $1b_1$, and $2a_1$ are not listed.
[e]For each of the *dominant* spin-adapted determinants that contribute to the 1^1A_1 and 2^1A_1 wave functions of O_3, the valence orbitals $3a_1$, $2b_1$, and $4a_1$ are all doubly occupied and therefore not listed. However, the *full* CAS(18,12) space also contains determinants that involve excitations from orbitals $3a_1$, $2b_1$, and $4a_1$.
[f]Indicated as shaded part are the active orbitals, $4b_1$ and $2b_2$, that have different occupations in $|D_1\rangle$ and $|D_2\rangle$.
[g]Indicated in bold are the active orbitals, $6a_1$ and $1a_2$, that have different occupations in $|D_3\rangle$ and $|D_4\rangle$.
[h]Orbitals of a_1 and b_1 symmetry are σ-type orbitals. Orbitals of a_2 and b_2 symmetry are π-type orbitals.

TABLE IV. Occupations of the ORMAS orbital subspaces in the reference space and the excitation spaces for the four CI wave functions in which the 2s orbitals are treated as correlation active orbitals.[a]

Active space	Reference inactive correlation inactive	Reference inactive correlation active	Reference active correlation active	Virtual orbitals
CAS(18,12)	$1a_1$, $1b_1$, $2a_1$		$3a_1$, $2b_1$, $4a_1$, $5a_1$, $3b_1$, $1b_2$, $6a_1$, $1a_2$, $4b_1$, $2b_2$, $7a_1$, $5b_1$	$8a_1$, $6b_1$, etc.
Ref.	6		18	0
Ref. + SD	6		16-18	0-2
Ref. + SDT	6		15-18	0-3
Ref. + SDTQ	6		14-18	0-4
CAS(18,10)	$1a_1$, $1b_1$, $2a_1$		$3a_1$, $2b_1$, $4a_1$, $5a_1$, $3b_1$, $1b_2$, $6a_1$, $1a_2$, $4b_1$, $2b_2$	$7a_1$, $5b_1$, $8a_1$, $6b_1$, etc.
Ref.	6		18	0
Ref. + SD	6		16-18	0-2
Ref. + SDT	6		15-18	0-3
Ref. + SDTQ	6		14-18	0-4
CAS(6,4)	$1a_1$, $1b_1$, $2a_1$	$3a_1$, $2b_1$, $4a_1$, $5a_1$, $3b_1$, $1b_2$	$6a_1$, $1a_2$, $4b_1$, $2b_2$	$7a_1$, $5b_1$, $8a_1$, $6b_1$, etc.
Ref.	6	12	6	0
Ref. + SD	6	10-12	4-8	0-2
Ref. + SDT	6	9-12	3-8	0-3
Ref. + SDTQ	6	8-12	2-8	0-4
CAS(2,2)	$1a_1$, $1b_1$, $2a_1$	$3a_1$, $2b_1$, $4a_1$, $5a_1$, $3b_1$, $1b_2$, $6a_1$, $1a_2$	$4b_1$, $2b_2$	$7a_1$, $5b_1$, $8a_1$, $6b_1$, etc.
Ref.	6	16	2	0
Ref. + SD	6	14-16	0-4	0-2
Ref. + SDT	6	13-16	0-4	0-3
Ref. + SDTQ	6	12-16	0-4	0-4

[a]See Section IV B for detailed explanations.

orbitals will also be excited into the reference-active orbitals by SD-excitations. However, the weak MO group is again placed into the virtual space.

Table V lists the orbital spaces for four corresponding wave functions, in which the "2s-group" is inactive in the reference space and also with respect to correlation excitations, as follows:

- CAS(12,9)*: This wave function is similar to the CAS(18,12) wave function of the preceding paragraph. It differs by excluding the orbitals $3a_1$, $4a_1$, $2b_1$ of the "2s-group" from being active in the reference space and also from excitations into the virtual space.
- CAS(12,7)*: This wave function is similar to the preceding CAS(12,9)* wave function except that the "weak MO group" ($7a_1$, $5b_1$) is moved from the reference space into the virtual space. It can also be deduced from the CAS(18,10) of the preceding paragraph by excluding the orbitals of the "2s-group" from being active in the reference space as well as from excitations into the virtual space.
- CAS(6,4)*: This wave function differs from the CAS(6,4) wave function of the preceding paragraph in that the orbitals of the 2s-group are excluded from the correlating excitations.
- CAS(2,2)*: This wave function differs from the CAS(2,2) wave function of the preceding paragraph in that the orbitals of the 2s-group are excluded from the correlating excitations.

C. Exact calculations and CEEIS extrapolations

The orders of magnitude of the dimensions of the determinantal configuration spaces for the eight cases specified in Sec. IV B are listed in Table VI for the reference functions, for the reference + SD functions, for the reference + SDT functions, and for the reference + SDTQ functions. For the reference + SDT and the reference + SDTQ subspaces, the table also lists the number of determinants that are generated when only the first 30 or 40 virtual natural orbitals are used in the correlating CI calculations, which are the reduced spaces that are needed in the context of the CEEIS extrapolation. The full values are given in Table T1 of the supplementary material.[41] It should be noted that these dimensions correspond to A_1 symmetry.

The bold font in Table VI indicates dimensions for which the calculations would have been impractical or impossible on the available computational facilities. The italic font indicates calculations that were not made because they would have been of interest only in conjunction with some of the calculations indicated by bold font. These data show that calculations

TABLE V. Occupations of the ORMAS orbital subspaces in the reference space and the excitation spaces for the four CI wave functions in which the 2s orbitals are treated as correlation inactive doubly occupied orbitals.[a]

Active space	Reference inactive correlation inactive	Reference inactive correlation active	Reference active correlation active	Virtual orbitals
CAS(12,9)*	$1a_1$, $1b_1$, $2a_1$, $3a_1$, $2b_1$, $4a_1$		$5a_1$, $3b_1$, $1b_2$, $6a_1$, $1a_2$, $4b_1$, $2b_2$, $7a_1$, $5b_1$	$8a_1$, $6b_1$, etc.
Ref.	12		12	0
Ref. + SD	12		10-12	0-2
Ref. + SDT	12		9-12	0-3
Ref. + SDTQ	12		8-12	0-4
CAS(12,7)*	$1a_1$, $1b_1$, $2a_1$, $3a_1$, $2b_1$, $4a_1$		$5a_1$, $3b_1$, $1b_2$, $6a_1$, $1a_2$, $4b_1$, $2b_2$	$7a_1$, $5b_1$, $8a_1$, $6b_1$, etc.
Ref.	12		12	0
Ref. + SD	12		10-12	0-2
Ref. + SDT	12		9-12	0-3
Ref. + SDTQ	12		8-12	0-4
CAS(6,4)*	$1a_1$, $1b_1$, $2a_1$, $3a_1$, $2b_1$, $4a_1$	$5a_1$, $3b_1$, $1b_2$	$6a_1$, $1a_2$, $4b_1$, $2b_2$	$7a_1$, $5b_1$, $8a_1$, $6b_1$, etc.
Ref.	12	6	6	0
Ref. + SD	12	4-6	4-8	0-2
Ref. + SDT	12	3-6	3-8	0-3
Ref. + SDTQ	12	2-6	2-8	0-4
CAS(2,2)*	$1a_1$, $1b_1$, $2a_1$, $3a_1$, $2b_1$, $4a_1$	$5a_1$, $3b_1$, $1b_2$, $6a_1$, $1a_2$	$4b_1$, $2b_2$	$7a_1$, $5b_1$, $8a_1$, $6b_1$, etc.
Ref.	12	10	2	0
Ref. + SD	12	8-10	0-4	0-2
Ref. + SDT	12	7-10	0-4	0-3
Ref. + SDTQ	12	6-10	0-4	0-4

[a]See Section IV B for detailed explanations.

TABLE VI. Number of determinants generated for the reference, CISD, CISDT, and CISDTQ active spaces of A_1 symmetry, using different reference active spaces for ozone. The meaning of the italic and bold fonts is discussed in the text at the beginning of Section IV C. The parentheses (x) imply ($\times 10^x$).[a]

		Excitation level						
			Ref. + SDT			Ref. + SDTQ		
Reference active space	Ref.	Ref. + SD	$m = 30$	$m = 40$	$m = M$[b]	$m = 30$	$m = 40$	$m = M$[b]
Number of determinants generated when 2s excitations are included								
CAS(18,12)	1.2 (4)	5.9 (8)	*2.5 (9)*	**6.2 (9)**	**4.8 (10)**	**4.8 (10)**	**1.6 (11)**	**>2.5 (12)**[c]
CAS(18,10)	3.0 (1)	4.8 (6)	*4.0 (7)*	*9.6 (7)*	*6.9 (8)*	*1.3 (9)*	**4.3 (9)**	**>6.0 (10)**[c]
CAS(6,4)	4.0 (0)	2.5 (6)	*2.8 (7)*	*6.6 (7)*	*4.8 (8)*	*1.1 (9)*	**3.5 (9)**	**>5.0 (10)**[c]
CAS(2,2)	2.0 (0)	8.0 (5)	1.0 (7)	2.5 (7)	1.8 (8)	4.7 (8)	1.5 (9)	**2.1 (10)**
Number of determinants generated when 2s excitations are excluded								
CAS(12,9)*	1.8 (3)	3.7 (7)	*1.0 (8)*	*2.5 (8)*	*1.9 (9)*	*1.2 (9)*	**4.0 (9)**	**6.1 (10)**
CAS(12,7)*	1.3 (1)	1.0 (6)	5.5 (6)	1.3 (7)	9.3 (7)	1.1 (8)	3.5 (8)	**4.9 (9)**
CAS(6,4)*	4.0 (0)	8.4 (5)	5.1 (6)	1.2 (7)	8.7 (7)	1.1 (8)	3.5 (8)	**4.8 (9)**
CAS(2,2)*	2.0 (0)	3.2 (5)	2.5 (6)	6.0 (6)	4.3 (7)	6.7 (7)	2.1 (8)	2.9 (9)

[a]The exact values are listed in Table T2 of the supplementary material.[41]
[b]M = 77 for CAS(18,10), CAS(6,4), CAS(2,2), CAS(12,7)*, CAS(6,4)*, and CAS(2,2)* active spaces, the value of M = 75 for CAS(18,12) and CAS(12,9)*. See text in Section IV B.
[c]Estimated values.

up to the SDT level can be performed for most of these wave functions. On the other hand, for the cases CAS(18,12), CAS(18,10), CAS(6,4), and CAS(12,9)*, the SDTQ energies are beyond the available capabilities, even for the CEEIS extrapolation procedure.

In light of these observations, the following correlation calculations were performed at all five geometries:

- For all eight orbital space cases identified in Sec. IV B, the reference energies and the CISD energies were calculated.
- For the cases identified as CAS(2,2), CAS(2,2)*, CAS(6,4)*, and CAS(12,7)* in Sec. IV B, the CISDT energies were calculated exactly as well as by CEEIS extrapolation.
- For the cases CAS(2,2), CAS(2,2)*, CAS(6,4)*, and CAS(12,7)*, the CISDTQ energies were calculated by CEEIS extrapolation.

In addition, exact SDTQ energies were obtained for the CAS(2,2)* case at two geometries, viz., TS and CI. In all calculations, the valence orbitals were reoptimized for the respective reference spaces. An exception was made for the CAS(12,7)* case, which will be discussed at the end of Section VI B.

The results of these calculations are documented in the supplementary material.[41] In this material, Table T2 contains a list of the number m of orbitals (see Section II) that are used for the reduced virtual spaces in the various CEEIS procedures. The graphs in Figures F1 to F9 of the supplementary material document the linear relationships described in Section II, on which the CEEIS extrapolations are based for all cases. Tables T3–T12 of the supplementary material contain the exact and extrapolated energies obtained for all calculations.[41]

V. QUALITY OF THE CEEIS EXTRAPOLATIONS

The reliability of the various CEEIS extrapolations in the cases CAS(2,2), CAS(2,2)*, CAS(6,4)*, and CAS(12,7)*can be assessed from the data documented in Table VII.

According to what was said in Section IV C, the *actual errors* of the CEEIS extrapolations with respect to the exact calculations are available for the SDT calculations in these cases. They are listed in the first and fourth numerical data

TABLE VII. Errors and predicted uncertainties of the CEEIS extrapolations of the configuration interaction triple and quadruple excitation increments [with respect to several active spaces] for the 1^1A_1 and 2^1A_1 states of ozone, using the *cc–p*VTZ basis set, in mh.

		1^1A_1 State			2^1A_1 State		
	Geometry	$\Delta E(3)$ error[a]	$\Delta E(3)$ uncertainty[b]	$\Delta E(4)$ uncertainty[b]	$\Delta E(3)$ error[a]	$\Delta E(3)$ uncertainty[b]	$\Delta E(4)$ uncertainty[b]
OM	CAS(2,2)	0.02	±0.64	±0.08	0.40	±0.53	±0.32
	CAS(2,2)*	−1.01	±0.49	±0.18	−1.82	±0.27	±0.08
	CAS(6,4)*	−1.28	±0.03	±0.04	−0.44	±0.29	±0.15
	CAS(12,7)*a	−0.87	±0.20	±0.02	0.30	±0.39	±0.04
	CAS(12,7)*b	−1.36	±0.23	±0.06	−0.36	±0.65	±0.17
TS	CAS(2,2)	−0.18	±1.31	±0.04	−1.33	±1.81	±1.78
	CAS(2,2)*	−1.31	±0.81	±0.42[c]	−1.58	±0.86	±0.11[c]
	CAS(6,4)*	−1.28	±0.79	±0.15	−1.87	±0.74	±0.17
	CAS(12,7)*a	−0.03	±0.13	±0.05	−0.09	±0.38	±0.02
	CAS(12,7)*b	−2.42	±1.43	±0.44	−0.65	±0.45	±0.05
XM	CAS(2,2)	−0.89	±1.55	±0.58	0.94	±2.12	±1.12
	CAS(2,2)*	−1.30	±0.82	±0.49	−1.59	±0.85	±0.18
	CAS(6,4)*	−1.33	±0.79	±0.04	−1.82	±0.73	±0.27
	CAS(12,7)*a	−0.03	±0.14	±0.05	−0.09	±0.38	±0.02
	CAS(12,7)*b	−3.38	±1.44	±0.23	0.27	±0.44	±0.26
CI	CAS(2,2)	−0.29	±1.91	±0.36	0.17	±1.59	±0.34
	CAS(2,2)*	−1.45	±1.06	±0.79[d]	−2.04	±0.91	±0.46[d]
	CAS(6,4)*	−0.19	±1.21	±0.17	−0.53	±1.36	±0.58
	CAS(12,7)*a	0.21	±0.25	±0.02	0.004	±0.41	±0.005
	CAS(12,7)*b	1.07	±3.41	±0.82	−2.04	±0.11	±0.18
RM	CAS(2,2)	−0.21	±0.64	±0.42	1.53	±2.24	±0.06
	CAS(2,2)*	−1.29	±0.47	±0.02	0.54	±0.58	±0.81
	CAS(6,4)*	−0.94	±0.57	±0.05	−2.83	±0.02	±0.06
	CAS(12,7)*a	−0.35	±0.57	±0.02	−3.41	±0.79	±0.24
	CAS(12,7)*b	−0.71	±1.47	±0.11	6.09	±0.24	±0.13

[a]The difference (Extrapolated Value − Exact Value).

[b]Uncertainties using the algorithm described in Section III B 4 of Ref. 34(a).

[c]For this case, exact values were also obtained. The differences (Extrapolated Values − Exact Values) are 0.40 mh and 0.52 mh for the 1^1A_1 and 2^1A_1 states, respectively.

[d]For this case, exact values were also obtained. The differences (Extrapolated Values − Exact Values) are 0.41 mh and −1.19 mh for the 1^1A_1 and 2^1A_1 states, respectively.

columns of Table VII for the 1^1A_1 and 2^1A_1 states, respectively. The second and fifth numerical data columns list the *predicted uncertainties* for the respective SDT extrapolations, which were obtained using the algorithm described in Section III B 4 of Ref. 34(a). (Of the two options given there, the more conservative estimate was used.) It is seen that, for the CAS(2,2) case, all of the actual errors are less than the estimated uncertainties. Most of the actual errors for the CAS(12,7)* case are also lower than the predicted uncertainties. (The difference between CAS(12,7)*a and CAS(12,7)*b in Table VII will be discussed in Section VI A.) For the CAS(2,2)* and CAS(6,4)* cases, on the other hand, the actual errors are somewhat larger than the predicted uncertainties. With very few exceptions, the actual error is less than 1.5 mh. Only for the 2^1A_1 state at the ring minimum, some errors are about 3 mh.

The predicted uncertainties of the extrapolated CISDTQ energies are listed in the third and sixth numerical data columns of Table VII for the 1^1A_1 and 2^1A_1 states, respectively. In view of the results found for the CISDT calculations, the actual errors of the $\Delta E(4)$ increments predicted for the CAS(2,2) and CAS(12,7)* cases are likely to be smaller than the listed predicted uncertainties. For the cases CAS(2,2)* and CAS(6,4)*, on the other hand, it is possible that the actual errors of the extrapolated $\Delta E(4)$ values are somewhat larger than the listed uncertainties. However, as mentioned in Section II, in all past experiences, the extrapolation of ΔE(4) *versus* ΔE(1,2) has consistently converged considerably more rapidly than the extrapolation of ΔE(3) *versus* ΔE(1,2). In view of the small errors that are observed for the extrapolation of the CISDT energies, it seems thus likely that the CISDTQ energies that are extrapolated for the CAS(2,2)* and CAS(6,4)* active spaces should lie within 1.5 mh of the exact values (except possibly for the values of the 2^1A_1 state at the ring minimum). These conclusions are supported by the results for the CISDTQ energies of the CAS(2,2)* case at the TS and CI geometries where, as mentioned in Section IV C, *exact* CISDTQ energies were calculated for both states. As noted in footnotes c and d of Table VII, the CEEIS extrapolated CISDTQ energies for the 1^1A_1 and 2^1A_1 states deviate from the exact values by 0.40 mh and −0.52 mh, respectively, at the TS geometry and by 0.41 mh and −1.19 mh, respectively, at the CI geometry.

In summary, the discussed deviations and the graphs in Figures F1 to F9 of the supplementary material[41] demonstrate that the linear relationships, which are the basis of the CEEIS extrapolations, remain valid under the severe present conditions, viz., the simultaneous extrapolations of two states in a molecule of three closely interacting atoms. Even for the 2^1A_1 state at the ring minimum, which lies more than 200 mh higher than the 1^1A_1 state, the discrepancy reaches 3 mh only for two data points in Table VII. The savings of the CEEIS procedure are apparent for the increments $\Delta(4)$ = (CISDTQ–CISDT), some with values up to 90 mh, which

TABLE VIII. Convergence of correlation increments for the energy of the 1^1A_1 state, in mh.

Geometry		$\Delta E(1,2)$	$\Delta E(3)$	$\Delta E(4)$[a]	ΔE_{Corr}[a,b]	Uncertainty
OM	CAS(2,2)	−682.43	−53.26	−79.32	−815.00	±0.08
	CAS(2,2)*	−449.79	−39.65	−36.17	−525.62	±0.18
	CAS(6,4)*	−363.31	−28.36	−18.17	−409.83	±0.04
	CAS(12,7)*a	−303.43	−16.28	−10.12	−329.83	±0.02
	CAS(12,7)*b	−365.19	−26.90	−15.45	−407.54	±0.06
TS	CAS(2,2)	−662.26	−52.56	−87.59	−802.41	±0.04
	CAS(2,2)*	−436.18	−39.11	−43.64 (−44.03)	−518.93 (−519.32)	±0.42
	CAS(6,4)*	−352.25	−18.15	−23.59	−394.00	±0.15
	CAS(12,7)*a	−289.63	−9.97	−11.26	−310.86	±0.05
	CAS(12,7)*b	−352.36	−18.86	−21.62	−392.84	±0.44
XM	CAS(2,2)	−662.28	−52.68	−88.35	−803.31	±0.58
	CAS(2,2)*	−436.20	−39.26	−44.03	−519.50	±0.49
	CAS(6,4)*	−352.08	−18.16	−24.09	−394.33	±0.04
	CAS(12,7)*a	−289.68	−9.97	−11.27	−310.92	±0.05
	CAS(12,7)*b	−352.19	−19.45	−20.79	−392.43	±0.23
CI	CAS(2,2)	−665.44	−57.91	−94.39	−817.73	±0.36
	CAS(2,2)*	−443.60	−44.90	−48.95 (−49.36)	−537.45 (−537.87)	±0.79
	CAS(6,4)*	−358.96	−18.97	−25.63	−403.55	±0.17
	CAS(12,7)*a	−288.63	−9.84	−11.65	−310.12	±0.02
	CAS(12,7)*b	−359.13	−20.24	−25.22	−404.60	±0.82
RM	CAS(2,2)	−652.96	−41.05	−77.17	−771.18	±0.42
	CAS(2,2)*	−420.66	−27.58	−34.01	−482.25	±0.02
	CAS(6,4)*	−385.80	−24.83	−23.26	−433.89	±0.05
	CAS(12,7)*a	−318.10	−14.44	−12.19	−344.74	±0.02
	CAS(12,7)*b	−384.84	−25.12	−21.59	−431.54	±0.11

[a]The values without parentheses were obtained using the CEEIS extrapolation for the CISDTQ increment $\Delta E(4)$. The values in parentheses for the CAS(2,2)* case at the TS and CI geometries were obtained by exact calculation of $\Delta E(4)$.
[b]Total correlation energies (up to SDTQ) relative to the respective reference states.

were typically recovered with millihartree accuracy by using only 40 of the 77 virtual orbitals, requiring less than 10% of the total number of determinants.

VI. CONVERGENCE OF CONFIGURATION INTERACTION EXPANSIONS

A. Rate of convergence with respect to increasing excitation levels

Tables VIII and IX list the incremental amounts of correlation energy that are, respectively, recovered in all cases for which the SDT and SDTQ excitations were calculated, viz., CAS(2,2), CAS(2,2)*, CAS(6,4)*, and CAS(12,7)*. Table VIII lists the increments due to the successive additions of single, double, triple, and quadruple excitations to the reference spaces for the 1^1A_1 state. Table IX lists the values for the 2^1A_1 state. (The difference between CAS(12,7)*a and CAS(12,7)*b in these tables is discussed below in this section.) For both states, the following implications regarding the rate of convergence with increasing excitation levels to the full CI energy are apparent.

- At all excitation levels, the magnitudes of the increments decrease in the order: CAS(2,2), CAS(2,2)*, CAS(6,4)*, and CAS(12,7)*.
- The rate of convergence depends markedly on the initial reference space.
- Convergence to millihartree accuracy has not yet been reached at the SDTQ level.

The first of these observations reflects the increasing effectiveness of the reference space. The other two observations contrast with the results found in diatomic molecules. In F_2, for instance,[42] the quintuple and sextuple excitations contributed less than a millihartree, and the convergence was found to be nearly the same for both the full valence CAS(14,8) reference space and for a reduced two-determinant CAS(2,2) reference space.

Since the CAS(2,2)*, CAS(6,4)*, and CAS(12,7)* calculations are all based on the same correlation active reference and virtual orbitals, they should yield the same total energy when sufficient excitations are included, namely, the full CI value for the case that the excitations from the 2s orbitals are excluded. Table X exhibits how close the present expansions up to quadruple excitations come to achieving this agreement for the two states. Each entry in this table corresponds to the wave function specified by the column header [CAS(6,4)* or CAS(12,7)*] and the excitation level specified for the row. Each entry lists the difference between the so specified energy and the corresponding energy of the CAS(2,2)* wave function.

For the CAS(12,7)* case, two kinds of calculations are listed as follows.

CAS(12,7)*-a: Following the usual procedure, the optimized orbitals for the CAS(12,7)* reference space are

TABLE IX. Convergence of correlation increments for the energy of the 2^1A_1 state, in mh.

Geometry		$\Delta E(1,2)$	$\Delta E(3)$	$\Delta E(4)$[a]	ΔE_{Corr}[a,b]	*Uncertainty*
OM	CAS(2,2)	−663.40	−55.78	−122.76	−841.95	±0.32
	CAS(2,2)*	−437.30	−50.07	−68.15	−555.52	±0.08
	CAS(6,4)*	−324.10	−13.62	−17.66	−355.38	±0.04
	CAS(12,7)*a	−270.89	−7.77	−10.62	−289.28	±0.02
	CAS(12,7)*b	−324.81	−13.29	−17.18	−355.28	±0.17
TS	CAS(2,2)	−707.75	−62.72	−107.60	−878.07	±1.78
	CAS(2,2)*	−488.57	−51.85	−58.30 (−57.78)	−598.72 (−598.20)	±0.11
	CAS(6,4)*	−361.07	−26.71	−26.05	−413.82	±0.15
	CAS(12,7)*a	−295.48	−12.02	−11.69	−319.19	±0.05
	CAS(12,7)*b	−365.01	−26.50	−23.13	−414.64	±0.05
XM	CAS(2,2)	−707.67	−62.61	−104.06	−874.34	±1.12
	CAS(2,2)*	−488.44	−51.69	−57.89	−598.03	±0.18
	CAS(6,4)*	−361.07	−26.70	−25.55	−413.32	±0.04
	CAS(12,7)*a	−295.64	−12.06	−11.69	−319.38	±0.05
	CAS(12,7)*b	−365.01	−25.91	−23.89	−414.81	±0.26
CI	CAS(2,2)	−715.68	−68.07	−112.27	−896.01	±0.35
	CAS(2,2)*	−500.25	−57.72	−65.41 (−64.22)	−623.37 (−622.18)	±0.46
	CAS(6,4)*	−365.55	−26.80	−31.10	−423.44	±0.17
	CAS(12,7)*a	−293.39	−11.71	−12.07	−317.16	±0.02
	CAS(12,7)*b	−369.37	−26.85	−26.32	−422.53	±0.18
RM	CAS(2,2)	−692.63	−80.91	−91.56	−865.11	±0.07
	CAS(2,2)*	−468.81	−68.31	−51.85	−588.97	±0.81
	CAS(6,4)*	−374.37	−35.16	−30.30	−439.83	±0.05
	CAS(12,7)*a	−317.17	−32.77	−24.02	−373.96	±0.24
	CAS(12,7)*b	−367.93	−42.62	−28.34	−438.89	±0.13

[a]The values without parentheses were obtained using the CEEIS extrapolation for the CISDTQ increment $\Delta E(4)$. The values in parentheses for the CAS(2,2)* case at the TS and CI geometries were obtained by exact calculation of $\Delta E(4)$.
[b]Total correlation energies (up to SDTQ) relative to the respective reference states.

TABLE X. The energy differences {E[CAS(6,4)*] − E[CAS(2,2)*]}and {E[CAS(12,7)*] − E[CAS(2,2)*]}at various excitation levels for the 1^1A_1 state and the 2^1A_1 state.[a]

		1^1A_1 energy differences (mh)			2^1A_1 energy differences (mh)		
	Geometry	CAS(6,4)*	CAS(12,7)*a	CAS(12,7)*b	CAS(6,4)*	CAS(12,7)*a	CAS(12,7)*b
OM	Ref.	−116.77	−120.11	−119.23	−214.94	−214.77	−215.04
	Ref. + SD	−30.29	26.25	−34.62	−101.75	−48.36	−102.54
	Ref. + SDT	−19.00	49.62	−21.87	−65.29	−6.05	−65.76
	Ref. + SDTQ[b]	−0.99	75.68	−1.15	−14.80	51.48	−14.79
TS	Ref.	−133.29	−134.52	−133.44	−192.86	−193.42	−193.34
	Ref. + SD	−49.36	12.02	−49.62	−65.36	−0.33	−69.78
	Ref. + SDT	−28.40	41.17	−29.37	−40.21	39.50	−44.43
	Ref. + SDTQ[b]	−8.36	73.55	−7.35	−7.96	86.11	−9.26
		(−7.96)[c]	(73.94)[c]	(−6.96)[c]	(−8.48)[c]	(85.59)[c]	(−9.78)[c]
XM	Ref.	−133.56	−134.79	−133.71	−192.63	−193.19	−193.11
	Ref. + SD	−49.44	11.74	−49.69	−65.25	−0.39	−69.68
	Ref. + SDT	−28.33	41.03	−29.88	−40.26	39.25	−43.90
	Ref. + SDTQ[b]	−8.39	73.79	−6.64	−7.92	85.45	−9.90
CI	Ref.	−142.49	−143.54	−142.59	−210.72	−211.09	−211.03
	Ref. + SD	−57.85	11.44	−58.12	−76.02	−4.23	−80.15
	Ref. + SDT	−31.91	46.49	−33.46	−45.10	41.78	−49.28
	Ref. + SDTQ[b]	−8.59	82.80	−9.74	−10.79	95.12	−10.18
		(−8.18)[c]	(84.21)[c]	(−9.32)[c]	(−11.98)[c]	(93.93)[c]	(−11.38)[c]
RM	Ref.	−56.28	−59.76	−58.69	−164.39	−166.14	−164.81
	Ref. + SD	−21.41	42.80	−22.87	−69.96	−14.50	−71.77
	Ref. + SDT	−18.67	55.93	−20.41	−36.80	21.04	−38.24
	Ref. + SDTQ[b]	−7.91	77.75	−7.99	−15.26	51.70	−14.73

[a]The difference between CAS(12,7)*a and CAS(12,7)*b is discussed in Section VI A.
[b]In these rows, all SDTQ energies were obtained by the CEEIS extrapolation.
[c]The energy differences reported in parentheses were obtained using exact CAS(2,2)* energies.

determined and used for generating the reference energy and the excitation increments.

CAS(12,7)*-b: The orbitals optimized for the CAS(6,4)* calculations were used to generate the reference functions and the excited configurations for the CAS(12,7)* calculations. This is also indicated in the headers of Table X. The reason for considering the alternative choice (b) will become apparent presently.

It is seen from Table X that, at all geometries, the energies of the CAS(12,7)-b *reference* wave functions are only about 1 mh higher than the energies of the respective CAS(12,7)*-a *reference* wave functions. However, a very different behavior is found for the energy increments due to the SD, SDT, and SDTQ excitations.

Consider first the CAS(12,7)*-b case. It is apparent that, in both states, the deviations of the CAS(12,7)*-b increments as well as those of the CAS(6,4)* increments from the CAS(2,2)* increments decrease successively and markedly with increasing excitations. At the SDTQ level, the deviations are between 1 and 8 mh for the 1^1A_1 state and between 8 and 15 mh for the 2^1A_1 state. These deviations between the different wave functions can be taken as a rough estimate of the order of magnitude of the deviation from the full CI limit in the absence of excitations from the 2s orbitals. One may thus expect that this full CI energy differs by less than a millihartree from the energy at the sextuple excitation level.

In contrast, the energies of the CAS(12,7)*-a calculations in Table X are seen to differ greatly from those of the CAS(2,2)* calculations (as well as from the CAS(12,7)*-b calculations). While the CAS(12,7)*-a *reference* energies are between 60 and 200 mh lower than the corresponding CAS(2,2)* energies, the CAS(12,7)*-a SD energies lie in fact over 10 mh *higher* than the corresponding CAS(2,2)* energies, and this positive deviation increases to about 80 mh for the higher excitation. These data imply a *very* much slower convergence of the CAS(12,7)*-a excitation expansion. Closer investigation shows that the optimization of the CAS(12,7)* reference function leads to orbitals that are very different from those obtained for all other reference functions and manifestly very unfavorable for the convergence of the excitation expansion.

For this reason, all CAS(12,7)* results that are quoted and used in the following discussions are obtained by CAS(12,7)*-b type calculations, i.e., with the CAS(6,4)*-optimized orbitals.

B. Effect of the omission of excitations from the orbitals of the 2s group

The omission of excitations from the 2s orbitals is a widely used practice in correlation calculations involving oxygen. The present calculations allow an assessment of the effect ΔE of this omission for the following five cases:

TABLE XI. Energy differences due to the correlation of 2*s* orbitals in corresponding wave functions, i.e., $\Delta E = E$ (excluding excitations from the 2*s* orbitals) $-E$(including excitations from the 2*s* orbitals), in mh.

Geometry			Active space of the reference wave function			
			$\Delta E(2,2)$[a]	$\Delta E(6,4)$[b]	$\Delta E(12,7/18,10)$[c]	$\Delta E(12,9/18,12)$[d]
OM	Ref.	1^1A_1	0.00	0.00	1.03	10.35
		2^1A_1	0.00	0.00	0.04	14.79
	Ref. + SD	1^1A_1	232.64	243.72	247.58	238.61
		2^1A_1	226.10	250.56	252.15	246.42
TS	Ref.	1^1A_1	0.00	0.00	1.13	10.34
		2^1A_1	0.00	0.00	0.16	10.76
	Ref. + SD	1^1A_1	226.08	239.01	239.81	244.10
		2^1A_1	219.19	235.64	237.31	244.17
XM	Ref.	1^1A_1	0.00	0.00	1.12	9.95
		2^1A_1	0.00	0.00	0.16	11.15
	Ref. + SD	1^1A_1	226.07	239.04	239.80	243.98
		2^1A_1	219.22	235.65	237.29	244.25
CI	Ref.	1^1A_1	0.00	0.00	0.98	9.57
		2^1A_1	0.00	0.00	0.11	10.72
	Ref. + SD	1^1A_1	221.83	235.70	235.95	245.41
		2^1A_1	215.43	232.81	233.49	245.69
RM	Ref.	1^1A_1	0.00	0.00	1.55	13.38
		2^1A_1	0.00	0.00	1.99	10.47
	Ref. + SD	1^1A_1	232.30	234.13	215.67	244.71
		2^1A_1	223.83	235.80	218.17	247.35

[a]$\Delta E = E$[CAS(2,2)*] $-E$[CAS(2,2)].
[b]$\Delta E = E$[CAS(6,4)*] $-E$[CAS(6,4)].
[c]$\Delta E = E$[CAS(12,7)*] $-E$[CAS(18,10)], energies for the CAS(12,7)* calculations were determined using the CASSCF(6,4) optimized orbitals (see the end of Section VI A).
[d]$\Delta E = E$[CAS(12,9)*] $-E$[CAS(18,12)].

$\Delta E(2,2) = E$[CAS(2,2)*] $- E$[CAS(2,2)],
$\Delta E(6,4) = E$[CAS(6,4)*] $- E$[CAS(6,4)],
$\Delta E(12,7/18,10) = E$[CAS(12,7)*] $- E$[CAS(18,10)],
$\Delta E(12,9/18,12) = E$[CAS(12,9)*] $- E$[CAS(18,12)].

These differences are listed in Table XI for the reference functions and the SD excitations in both electronic states. Furthermore, Table XII lists the differences $\Delta E(2,2)$ for the SDT excitations and the SDTQ excitations.

The data in Table XI show that, within each *reference* space, the excitations from the 2s orbitals contribute very little. They lower the energy by about a millihartree or less in all cases except for the CAS(18,12), where this lowering is between 10 and 15 mh. However, at the SD level, the effect is more than an order of magnitude larger. It is approximately 220–230 mh for the CAS(2,2) case and about 240–250 mh for the other cases. The effect increases further for the SDT and SDTQ excitations, as shown in Table XII for the CAS(2,2) case, where these differences go up to around 280 mh.

Even though the magnitudes of these effects for the various reference choices are broadly similar at different geometries, the differences between the various reference choices are still sufficient so that marked differences between the various cases may also be expected when energy differences between different points on the potential energy surfaces are being calculated. This matter is discussed in Section VII.

TABLE XII. Correlation contributions due to the 2s orbitals at the SDT and SDTQ levels in the CAS(2,2) function, i.e., the energy differences $\Delta E(2,2) = E$[CAS(2,2)*] $-E$[CAS(2,2)] $= E$(excluding excitations from the 2*s* orbitals) $-E$ (including excitations from the 2*s* orbitals), in mh.

Excitation level		Geometry				
		OM	TS[a]	XM	CI[a]	RM
Ref. + SDT	1^1A_1	246.25	239.53	239.49	234.84	245.77
	2^1A_1	231.81	230.06	230.14	225.78	236.43
Ref. + SDTQ	1^1A_1	289.39	283.49 (283.09)	283.81	280.28 (279.87)	288.93
	2^1A_1	286.43	279.35 (279.87)	276.31	272.64 (273.83)	276.14

[a]All SDTQ energies without parentheses were obtained by CEEIS extrapolation. The energy differences in parentheses were obtained using exact CAS(2,2)* energies.

TABLE XIII. Changes in the energies of the 1^1A_1 state and the 2^1A_1 state due to moving the $7a_1$ and $5b_1$ orbitals from the reference space to the virtual space, in mh.

		1^1A_1 State		2^1A_1 State	
		CAS(12,7)*[a]	CAS(18,10)[b]	CAS(12,7)*[a]	CAS(18,10)[b]
Geometry		Excluding 2*s* excitations	Including 2*s* excitations	Excluding 2*s* excitations	Including 2*s* excitations
OM	Ref.	133.99	143.31	75.61	90.36
	Ref + SD	60.40	51.43	39.51	33.78
	Ref + SDT	44.75		36.60	
TS	Ref.	115.99	125.20	137.18	147.78
	Ref + SD	45.42	49.70	53.58	60.44
	Ref + SDT	37.31		37.70	
XM	Ref.	116.70	125.53	136.28	147.27
	Ref + SD	46.09	50.26	52.92	59.88
	Ref + SDT	37.43		37.60	
CI	Ref.	129.86	138.44	146.96	157.57
	Ref + SD	47.47	56.93	54.56	66.76
	Ref + SDT	37.83		38.12	
RM	Ref.	145.12	156.96	155.01	163.48
	Ref + SD	48.80	77.84	67.79	96.98
	Ref + SDT	34.61		44.67	

[a]$\Delta E = E$[CAS(12,7)*] $-E$[CAS(12,9)]. Energies for the CAS(12,7)* calculations were determined using the CASSCF(6,4) optimized orbitals (see the end of Section VI A).
[b]$\Delta E = E$[CAS(18,10)*] $-E$[CAS(18,12)].

TABLE XIV. Energy differences for the 1^1A_1 state, in mh, relative to the energy of this state at its open minimum (OM).

		Active space of the reference wave function							
		CAS(2,2)* Excluding 2*s* excitations	CAS(2,2) Including 2*s* excitations	CAS(6,4)* Excluding 2*s* excitations	CAS(6,4) Including 2*s* excitations	CAS(12,7)*[a] Including 2*s* excitations	CAS(18,10) Including 2*s* excitations	CAS(12,9)* Excluding 2*s* excitations	CAS(18,12) Including 2*s* excitations
Geometry									
ΔTS	Ref.	80.30	80.30	63.78	63.78	66.09	65.99	84.09	84.10
	Ref. + SD	93.92	100.48	74.84	79.56	78.92	86.69	93.91	88.42
	Ref. + SDT	94.46	101.17	85.05		86.96		94.40	
	Ref. + SDTQ[b]	86.99 (86.60)[b]	92.89	79.62		80.79			
ΔXM	Ref.	80.61	80.61	63.81	63.81	66.12	66.03	83.41	83.81
	Ref. + SD	94.19	100.76	75.05	79.73	79.12	86.90	93.44	88.07
	Ref. + SDT	94.58	101.34	85.25		86.58		93.90	
	Ref. + SDTQ[b]	86.72	92.30	79.32		81.24			
ΔCI	Ref.	105.80	105.80	80.08	80.08	82.43	82.48	86.56	87.35
	Ref. + SD	111.99	122.80	84.43	92.45	88.49	100.13	101.43	94.63
	Ref. + SDT	106.74	118.15	93.82		95.15		102.08	
	Ref. + SDTQ[b]	93.97 (93.55)[b]	103.08	86.36		85.38			
ΔRM	Ref.	1.22	1.22	61.72	61.72	61.76	61.24	50.62	47.59
	Ref. + SD	30.35	30.70	39.23	48.83	42.11	74.02	53.71	47.61
	Ref. + SDT	42.43	42.91	42.76		43.89		54.03	
	Ref. + SDTQ[b]	44.59	45.05	37.67		37.76			

[a]Energies for the CAS(12,7)* calculations were determined using the CASSCF(6,4) optimized orbitals (see the end of Section VI A).
[b]The SDTQ values without parentheses were obtained using the CEEIS extrapolation for the CISDTQ increments. The values in parentheses for CAS(2,2)* were obtained by exact CISDTQ calculations.

C. Effect of moving the weak MO group (orbitals $7a_1$ and $5b_1$) from the reference space into the virtual space

Since the valence orbitals $7a_1$ and $5b_1$ have occupations of less than 0.2 in the full valence space CAS wave function, the expectation is that moving them from the reference space into the virtual space, and then occupying and exciting them successively in the context of the general SD, SDT, and SDTQ excitations, will adequately recover the relevant reference and correlation contributions from this weak MO group. By comparison, in the F_2 molecule,[42] it was found that similar orbital moves increased the energy at the SDTQ level by less than 0.5 mh.

The present calculations allow an assessment of the effect of this "weak MO move" on the reference energies and the SD excitation energies of the following two cases:

$\Delta E(12,9) = E[\mathrm{CAS}(12,7)^*] - E[\mathrm{CAS}(12,9)^*]$,

$\Delta E(18,12) = E[\mathrm{CAS}(18,10)] - E[\mathrm{CAS}(18,12)]$.

These differences are listed in Table XIII for both states. Notwithstanding the small occupations in the full valence space, the move of these orbitals is seen to increase all reference energies by over 100 mh. However, at the SD level, these energy differences have markedly decreased. Their magnitudes are then about half an order of magnitude smaller than the total SD correlation increments and rather comparable to the total SDT correlation increments (see Table IX). It is therefore justified to expect that at the excitation level where the CI expansions approach the full CI energy to a fraction of a millihartree (presumably sextuple excitations, see Section VI A), the effect of the weak MO move will be no larger.

VII. ENERGY DIFFERENCES ON THE POTENTIAL ENERGY SURFACES

A universal objective of quantum chemistry is the identification of electronic wave functions that are capable of generating useful predictions of relevant chemical or physical energy *changes* because the errors in the individual energies cancel out when the energy *differences* are calculated. In view of the considerable deviations that were found between the various CI approaches to the correlation energy recovery in Sec. VI, the question arises whether these calculations nonetheless lead to quantitative conclusions regarding relevant energy *differences* on the two potential energy surfaces. Tables XIV and XV contain the pertinent data.

Table XIV lists the values that are obtained by the various calculations for the following energy differences on the 1^1A_1 surface:

ΔRM = The energy elevation of the ring minimum over the open minimum = $[E(\mathrm{RM}) - E(\mathrm{OM})]$,

ΔTS = The barrier height relative to the open minimum = $[E(\mathrm{TS}) - E(\mathrm{OM})]$,

TABLE XV. Excitation energy differences $[E(2^1A_1) - E(1^1A_1)]$, in mh.

		Active space of the reference wave function							
	Geometry	CAS(2,2)* Excluding 2*s* excitations	CAS(2,2) Including 2*s* excitations	CAS(6,4)* Excluding 2*s* excitations	CAS(6,4) Including 2*s* excitations	CAS(12,7)*[a] Excluding 2s excitations	CAS(18,10) Including 2*s* excitations	CAS(12,9)* Excluding 2*s* excitations	CAS(18,12) Including 2*s* excitations
OM	Ref.	194.38	194.38	96.21	96.21	98.57	99.56	156.95	152.51
	Ref. + SD	206.88	213.42	135.42	128.59	138.95	134.38	159.85	152.04
	Ref. + SDT	196.45	210.89	150.16		152.57		160.72	
	Ref. + SDTQ[b]	164.48	167.44	150.67		150.84			
TS	Ref.	82.21	82.21	22.64	22.64	22.31	23.28	1.12	0.70
	Ref. + SD	29.82	36.72	13.83	17.19	9.66	12.16	1.50	1.43
	Ref. + SDT	17.08	26.56	5.27		2.02		1.63	
	Ref. + SDTQ[b]	2.42 (3.34)[b]	6.56	2.82		0.51			
XM	Ref.	80.92	80.92	21.85	21.85	21.51	22.47	1.94	0.74
	Ref. + SD	28.68	35.53	12.86	16.25	8.69	11.20	1.86	1.58
	Ref. + SDT	16.25	25.60	4.32		2.23		2.06	
	Ref. + SDTQ[b]	2.39	9.89	2.86		−0.87			
CI	Ref.	86.94	86.94	18.71	18.71	18.51	19.37	1.40	0.25
	Ref. + SD	30.30	36.70	12.13	15.02	8.27	10.73	1.17	0.89
	Ref. + SDT	17.48	26.54	4.29		1.66		1.37	
	Ref. + SDTQ[b]	1.02 (2.62)[b]	8.66	−1.18		0.57			
RM	Ref.	402.51	402.51	294.39	294.39	296.40	295.95	286.51	289.42
	Ref. + SD	354.36	362.83	305.81	304.14	305.46	302.97	286.47	283.83
	Ref. + SDT	313.62	322.97	295.49		295.80		285.75	
	Ref. + SDTQ[b]	295.79	308.58	288.44		289.04			

[a]Energies for the CAS(12,7)* calculations were determined using the CASSCF(6,4) optimized orbitals (see the end of Section VI A).

[b]The SDTQ values without parentheses were obtained using the CEEIS extrapolation for the CISDTQ increments. The values in parentheses for CAS(2,2)* were obtained by exact CISDTQ calculations.

ΔXM = The elevation of the $1A_1$ state energy at the 2^1A_1 state minimum over the open minimum = [E(XM) − E(OM)],

ΔCI = The elevation of the $1A_1$ state energy at the conical intersection over the open minimum = [E(CI) − E(OM)].

For the *ring minimum elevation ΔRM*, the SDTQ calculations of the CAS(2,2), CAS(2,2)*, CAS(6,4)*, and CAS(12,7)* models are seen to give, respectively, the values 45, 45, 38, and 38 mh, while the SD calculations of the CAS(6,4), CAS(12,7)*, CAS(12,9)*, and CAS(18,12) models yield the respective values 49, 42, 54, and 48 mh. For the *barrier height ΔTS*, the SDTQ calculations of the CAS(2,2), CAS(2,2)*, CAS(6,4)*, and CAS(12,7)* models give, respectively, 93, 87, 80, and 81 mh, while the SD calculations of the CAS(6,4), CAS(18,10), CAS(12,9)*, and CAS(18,12) models yield the respective values 80, 87, 94, and 88 mh. From these results, one would infer that the ring minimum lies about 45–50 mh above the open minimum, that the barrier lies about 85–90 mh above the open minimum, and that the barrier lies about 40–45 mh above the ring minimum. At the *geometry of the minimum of the* 2^1A_1 *state*, the energy of the 1^1A_1 state differs by less than a millihartree from the energy at the transition state in all calculations. At the *conical intersection geometry,* the elevation of the 1^1A_1 state above the transition state is found to be between 7 and 13 mh.

Table XV lists the excitation energies [E(2^1A_1) − E(1^1A_1)] at all five geometries. For the geometries TS, XM, and CI, where the two states come close to each other, the various calculations yield energy differences that vary between 1 and 15 mh. At the CI geometry, the difference is 1 mh for four wave functions and 5–15 mh for the other four. Since CI is the intersection geometry for the full valence CAS(18,12) reference functions, the implication is that, in some cases, the location of the intersection has somewhat shifted. At the open minimum, the excitation energy from the 1^1A_1 state to the 2^1A_2 state varies between 130 and 170 mh for the different wave functions. At the ring minimum, the excitation energy varies between 270 and 310 mh. It should be noted that, at this geometry, four other states lie between 1^1A_1 and 2^1A_1. The accurate calculation of the large excitations is manifestly more difficult.

Tables XIV and XV also allow an assessment of how much the energy differences are affected by the omission of the excitations from the 2s-type reference orbitals that were discussed in Section VI B, viz., ΔE(2,2), ΔE(6,4), ΔE(12,7/18,10), and ΔE(12,9/18,12). The data in Table XIV show that, at the SD excitation level, this omission changes the energy differences on the 1^1A_1 surface by amounts between −6 and +8 mh. Table XV shows that, at the SD level, the corresponding excitation energies change by amounts between −10 and +10 mh (except for the ring minimum where the CAS(6,4) change is 20 mh). The values for the CAS(2,2) and CAS(2,2)* cases furthermore show that there is no significant difference between the SD and the SDTQ levels regarding the effect of the omission of excitations from the 2s orbital group.

VIII. CONCLUSIONS

Valence correlated energies of the 1^1A_1 state and the 2^1A_1 state of ozone were calculated for five geometries that were determined at the full valence MCSCF [CAS(18,12)] level, viz., the geometries of the 1^1A_1 open minimum, the 1^1A_1 ring minimum, the transition state between these two minima, the minimum of the 2^1A_1 state, and the conical intersection between the two states. The strong interactions between the three close atoms and the two diabatic states generate a challenging problem in predicting accurate energies, for which experimental information so far exists only in the case of the 1^1A_1 open minimum.

Eight configuration interaction expansions, based on *cc-p*VTZ bases and differing in the reference spaces, were explored. For the four larger reference spaces, including the full valence space, the contributions of the SD excitations were calculated. For the other CI expansions, the contributions of the SD, SDT, and SDTQ excitations were obtained.

All SD contributions and SDT contributions as well as one of the SDTQ contributions were determined exactly and also by CEEIS extrapolation. The CEEIS method proved to be very accurate, using only 10% of the respective excited determinants. This method was then used to determine the SDTQ energies in the other three cases.

The examination of the CI expansions up to the quadruple excitations leads to the estimate that convergence to within about 1 mh of the full CI limit can be expected at the sextuple excitation level.

It was furthermore found that omission of the correlations of the 2s oxygen orbitals, which is a widely used approximation, causes uncertainties of about ±10 mh with respect to the energy differences on the 1^1A_1 surface and with respect to the excitation energies between the energy surfaces of the two states.

The present calculations lead to the estimate that the elevation of the ring minimum over the open minimum is between 45 and 50 mh and that the barrier between them is about 85–90 mh with respect to the open minimum. The excitation energy between the 1^1A_1 state and the 2^1A_1 state is estimated to be between 130 and 170 mh at the open minimum and between 270 and 310 mh at the ring minimum. In the region encompassing the geometries of the transition state, the excited state minimum, and the conical intersection [of the CAS(18,12) wave function], all of which lie close to each other, the difference between the two states varies between 1 and 10 mh, implying a shift in the conical intersection.

It is conceivable that SDTQ excitations with respect to the full CAS(18,12) valence space ($>10^{12}$ determinants) may approximate the full CI energy within less than a millihartree. But for any method that is based on a significantly reduced reference space, the values obtained by quadruple (or less) excitations are unlikely to approach the full CI value more reliably than has been found in the present study. Nor does it seem likely that observable energy differences can be ascertained more reliably. The results reported by Müller *et al.* in Ref. 22 support this inference.

ACKNOWLEDGMENTS

This work was supported by the US Department of Energy, Office of Basic Energy Sciences, Division of Chemical Sciences, Geosciences & Biosciences through the Ames

Laboratory at Iowa State University under Contract No. DE-AC02-07CH11358. In part (for J.I.), the work was also supported with federal funds from the National Cancer Institute, National Institutes of Health, under Contract No. HHSN 261200800001E. The content of this publication does not necessarily reflect the views or policies of the Department of Health and Human Services.

[1]J. A. Logan, J. Geophys. Res.: Atmos. **90**, 10463, doi:10.1029/JD090iD06p10463 (1985).
[2]S. O. Andersen, M. L. Halberstadt, and N. Borgford-Parnell, J. Air Waste Manage. Assoc. **63**, 607 (2013).
[3](a) D. Bermúdez-Aguirre and G. V. Barbosa-Cánovas, Food Control **29**, 82 (2012); (b) F. A. Miller, C. L. M. Silva, and T. R. S. Brandão, Food Eng. Rev. **5**, 77 (2013); (c) H. Lee, E. Lee, C.-H. Lee, and K. Lee, J. Ind. Eng. Chem. **17**, 468 (2011); (d) Y. Penru, A. R. Guastalli, S. Esplugas, and S. Baig, Ozone: Sci. Eng. **35**, 63 (2013).
[4](a) M. B. Rubin, Helv. Chim. Acta **86**, 930 (2003); (b) P. S. Bailey, Chem. Rev. **58**, 925 (1958); (c) W. P. Griffith, Coord. Chem. Rev. **219-221**, 259 (2001); (d) S. G. Van Ornum, R. M. Champeau, and R. Pariza, Chem. Rev. **106**, 2990 (2006).
[5](a) J. A. Joens, J. Geophys. Res. **91**, 14533 (1986); (b) J. R. Locker, J. A. Joens, and E. J. Bair, J. Photochem. **36**, 235 (1987); (c) H. Hippler, R. Rahn, and J. Troe, J. Chem. Phys. **93**, 6560 (1990).
[6](a) S. M. Anderson, P. Hupalo, and K. Mauersberger, J. Chem. Phys. **99**, 737 (1993); (b) S. M. Anderson and K. Mauersberger, J. Geophys. Research: Atmos. **100**, 3033 (1995); (c) A. Barbea, M.-R. De Backera, E. Starikovab, X. Thomasa, and Vl. G. Tyuterev, J. Quant. Spectrosc. Radiat. Transfer **149**, 51 (2014); (d) E. Starikova, A. Barbe, M.-R. De Backer, Vl. G. Tyuterev, D. Mondelain, S. Kassi, and A. Campargue, *ibid.* **149**, 211 (2014).
[7](a) D. G. Imre, J. L. Kinsey, and R. W. Field, J. Phys. Chem. **86**, 2564 (1982); (b) D. W. Arnold, C. Xu, E. H. Kim, and D. M. Neumark, J. Chem. Phys. **101**, 912 (1994); (c) K. M. Ervin and W. C. Lineberger, in *Advances in Gas Phase Ion Chemistry*, edited by N. G. Adams and L. M. Babcock (JAI Press, Greenwich, 1992), p. 121.
[8]T. Tsuneda, H. Nakano, and K. Hirao, J. Chem. Phys. **103**, 6520 (1995).
[9]A. Kalemos and A. Mavridis, J. Chem. Phys. **129**, 05312 (2008).
[10]P. Borowski, M. Fülscher, P. A. Malmquist, and B. O. Roos, Chem. Phys. Lett. **237**, 195 (1995).
[11]A. Banichevich and S. Peyerimhof, Chem. Phys. **174**, 93 (1993).
[12]L. Houston, in *Modern Trends in Chemical Reaction Dynamics: Experiment Theory (Part 2)*, edited by X. Yang and K. Liu (World Scientific, Singapore, 2004), Vol. 14.
[13]H. S. Johnston, Annu. Rev. Phys. Chem. **43**, 1 (1992).
[14]Y. Matsumi and M. Kawasaki, Chem. Rev. **103**, 4767 (2003).
[15](a) D. Picconi and S. Y. Grebenshchikov, J. Chem. Phys. **141**, 074311 (2014); (b) M. Braunstein and R. T Pack, *ibid.* **96**, 6378 (1992); (c) C. Woywod, M. Stengle, W. Domcke, H. Flöthmann, and R. Schinke, *ibid.* **107**, 7282 (1997); (d) P. J. Hay, R. T Pack, R. B. Walker, and E. J. Heller, J. Phys. Chem. **86**, 862 (1982); (e) K. Yamashita, K. Morokuma, F. Le Quéré, and C. Leforestier, Chem. Phys. Lett. **191**, 515 (1992).
[16](a) A. Perveaux, D. Lauvergnat, B. Lasorne, F. Gatti, M. A. Robb, G. J. Halász, and Á. Vibók, e-print physics.atm-clus (2014); (b) G. J. Halász, A. Perveaux, B. Lasorne, M. A. Robb, F. Gatti, and Á. Vibók, Phys. Rev. A **88**, 023425 (2013); (c) G. J. Halász, A. Perveaux, B. Lasorne, M. A. Robb, F. Gatti, and Á. Vibók, Phys. Rev. A **86**, 043426 (2012); (d) W. Domcke and C. Woywod, Chem. Phys. Lett. **216**, 362 (1993).
[17]R. Schinke and G. C. McBane, J. Chem. Phys. **132**, 044305 (2010).
[18](a) L. A. Curtiss, K. Raghavachari, G. W. Trucks, and J. A. Pople, J. Chem. Phys. **94**, 7221 (1991); (b) T. Helgaker, J. Gauss, P. Jørgensen, and J. Olsen, *ibid.* **106**, 6430 (1997); (c) D. Feller and D. A. Dixon, *ibid.* **115**, 3484 (2001); (d) K. Kowalski and P. Piecuch, *ibid.* **120**, 1715 (2004); (e) O. Hino, T. Kinoshita, G. K.-L. Chan, and R. J. Bartlett, *ibid.* **124**, 114311 (2006); (f) M. Okoshi and H. Nakai, J. Comput. Chem. **35**, 1473 (2014).
[19]M. K. Sprague and K. K. Irikura, Theor. Chem. Acc. **133**, 1544 (2014).
[20]P. J. Hay, T. H. Dunning, and W. A. Goddard, J. Chem. Phys. **63**, 3912 (1975).
[21]E. Miliordos and S. Xantheas, J. Am. Chem. Soc. **136**, 2808 (2014), and references therein.
[22]T. Müller, S. S. Xantheas, H. Dachsel, R. J. Harrison, J. Nieplocha, R. Shephard, G. S. Keziora, and H. Lischka, Chem. Phys. Lett. **293**, 72 (1998).
[23](a) R. Siebert, R. Schinke, and M. Bittererová, Phys. Chem. Chem. Phys. **3**, 1795 (2001); (b) R. Siebert, P. Fleurat-Lessard, R. Schinke, M. Bittererová, and S. C. Farantos, J. Chem. Phys. **116**, 9749 (2002).
[24]R. Dawes, P. Lolur, A. Li, B. Jiang, and H. Guo, J. Chem. Phys. **139**, 201103 (2013), and references therein.
[25]L. Meyer, *Modern Theories of Chemistry* (Longmans, London, 1888), p. 197.
[26](a) P. J. Hay and W. A. Goddard III, Chem. Phys. Lett. **14**, 46 (1972); (b) P. J. Hay, T. H. Dunning, and W. A. Goddard, *ibid.* **23**, 457 (1973); (c) J. S. Wright, Can. J. Chem. **51**, 139 (1973); (d) S. Shih, B. J. Buenker, and S. D. Peyerimhoff, Chem. Phys. Lett. **28**, 463 (1974).
[27](a) T. J. Lee, J. Chem. Phys. **93**, 489 (1990); (b) T. J. Lee, Chem. Phys. Lett. **169**, 529 (1990).
[28]Z.-W. Qu, H. Zhu, and R. Schinke, J. Chem. Phys. **123**, 204324 (2005).
[29](a) S. S. Xantheas, S. T. Elbert, and K. Ruedenberg, J. Chem. Phys. **93**, 7519 (1990); (b) S. S. Xantheas, G. J. Atchity, S. T. Elbert, and K. Ruedenberg, *ibid.* **94**, 8054 (1994); (c) G. J. Atchity and K. Ruedenberg, *ibid.* **99**, 3790 (1993).
[30](a) G. J. Atchity and K. Ruedenberg, Theor. Chem. Acc. **96**, 176 (1997); (b) G. J. Atchity, K. Ruedenberg, and A. Nanayakara, *ibid.* **96**, 195 (1997).
[31]J. Ivanic, G. J. Atchity, and K. Ruedenberg, J. Chem. Phys. **107**, 4307 (1997).
[32]B. Fleming, P. T. Wolczanski, and R. Hoffman, J. Am. Chem. Soc. **127**, 1278 (2005).
[33]L. De Vico, L. Pegado, J. Heimdal, P. Söderhjelm, and P. O. Roos, Chem. Phys. Lett. **461**, 136 (2008).
[34](a) K. Ruedenberg and L. Bytautas, J. Chem. Phys. **121**, 10905 (2004); (b) **121**, 10919 (2004); (c) **121**, 10852 (2004); (d) **122**, 154110 (2005); (e) **124**, 174304 (2006).
[35]L. Bytautas, N. Matsunaga, G. E. Scuseria, and K. Ruedenberg, J. Phys. Chem. A **116**, 1717 (2012).
[36]See, e.g., J. S. Boschen, D. Theis, K. Ruedenberg, and T. L. Windus, Theor. Chem. Acc. **133**, 1425 (2014).
[37]M. W. Schmidt, K. K. Baldridge, J. A. Boatz, S. T. Elbert, M. S. Gordon, J. H. Jensen, S. Koseki, N. Matsunaga, K. A. Nguyen, S. Su, T. L. Windus, and M. Dupuis, "General atomic and molecular electronic structure system," J. Comput. Chem. **14**, 1347 (1993).
[38]T. H. Dunning, J. Chem. Phys. **90**, 1007 (1989).
[39]G. Herzberg, *Electronic Spectra and Electronic Structure of Polyatomic Molecules* (Van Nostrand, New York, 1966).
[40]J. Ivanic, J. Chem. Phys. **119**, 9364 (2003); **119**, 9377 (2003).
[41]See supplementary material at http://dx.doi.org/10.1063/1.4942019, which contains all actual energies and documents the CEEIS extrapolations. It also contains detailed data regarding the CI spaces.
[42]L. Bytautas, T. Nagata, M. S. Gordon, and K. Ruedenberg, J. Chem. Phys. **127**, 164317 (2007).